UCLouvain

FACULTE DES SCIENCES

Faculté des sciences

Study of the mechanism inducing ferroelectricity in anti-Ruddelsden-Popper structures

Auteur·es : Louis Alaerts

Promoteur·rices : Geoffroy Hautier et Maksim Markov

Lecteur·rices : Janine George, Gian-Marco Rignanese et Yaroslav Filinchuk

Année académique 2019-2020

Acknowledgments

Foremost, I am particulary grateful for the help, the trust and the assistance given by Geoffroy, my promotor, not only during this last year, but also the year before. If I am here today, it is without a doubt thanks to him. The other person without whom I could never have achieved this master thesis is Maksim, my tutor. I specially thank him for all its explanations and its patience. I also warmly thank the other members of the lab that have contribute to this work.

I also thank my father for the corrections he brought and my mother for its support. I also want to make a special thanks to my grand-parents who have try their best to understand what this master thesis is about.

Abstract

Discovered in Rochelle salt in 1921 as a scientific curiosity, ferroelectricity has quickly started to attract the attention of researchers. Nowadays, ferroelectric materials are used in many technological applications such as actuators, piezoelectric sensors or memory elements. The possibility to couple ferroelectricity with ferromagnetism in magnetoelectric multiferroics further increase its attractiveness.

For a long time, many studies focused on perovskite oxides ABO_3 such as $BaTiO_3$ or $KNbO_3$ because of their simple structures. It allowed the development of valuable insights about ferroelectricity and led to important applications. However, this narrow focus limited the design and the optimization of material's properties and thus, their applications. The discovery of new ferroelectric materials and the subsequent comprehension of the mechanisms inducing ferroelectricity could greatly benefits to the field.

In this master thesis, we investigate the ferroelectric properties of Ba_4Sb_2O, a promising candidate recently discovered by our group, and compare it to $BaTiO_3$. Our analysis includes the study of the ferroelectric properties such as the polarization and the Born effective charges, the mechanism inducing ferroelectricity, a comparison with Ca_4Sb_2O and Sr_4Sb_2O and the behavior of Ba_4Sb_2O when subjected to stress.

The calculation of the polarization using the Born effective charges and the displacements gives us a value of 11.18 $\mu C/cm^2$ while the Berry phase approach leads to a value of 7.33 $\mu C/cm^2$. These values are comparable to the one found in $BaTiO_3$, where the polarization is around 27 and 36 $\mu C/cm^2$ depending on the phase considered.

We found that it is the hybridization of the O $2p$ states with the Ba $5d$ states that leads to the off-center displacement of the O and to the stabilization of the ferroelectric state. This situation is analogue to the one found in $BaTiO_3$ where it is the

hybridization of the Ti $3d$ states with the O $2p$ states that induces the ferroelectric distortion. Furthermore, we showed that the different behaviors of paraelectric Ca_4Sb_2O, antiferroelectric Sr_4Sb_2O and ferroelectric Ba_4Sb_2O are associated to the widening of the gap between the valence and the conductive bands.

From the strain analysis of Ba_4Sb_2O, we found that a compressive strain applied in the a, b plane could enhance the stability of the ferroelectric phase over the paraelectric phase while increasing the polarization.

Table of contents

Chapter 1

Introduction

Proposed in 1965, Moore's law states that the complexity of integrated circuits will double every two years [1]. This empirical law is still correct today. It explains why a smartphone smaller that fits in the palm of a hand is thousands of times more powerful than a 1960 mainframe computer the size of a room. The graphic representation of Moore's law (Fig 1.1) is an illustration of the spectacular growth of the electronic industry during the second part of the 20th century.

It represents the number of transistors carried by a microchip between 1970 and 2019. Thus, electronic devices became smaller and smaller resulting in an impressive drop of prices because a single chip could contain more and more transistors [2]. As a result, the computer market has experienced a rapid growth with appearance of personal computer in the seventies. The following decades witnessed the birth of the Internet and with it, information technologies, social networks, big data, etc. Nowadays, electronic devices are widespread. GPS are used instead of maps, telephones are replaced by smartphones, checks are abandoned to the profit of payment cards. Even entertainment is evolving with the apparition of online games. In other words, they have become an essential tool for everyday life. However, this spectacular technological progress has a cost that was almost invisible a few decades ago but which has now become noticeable, electric consumption.

Communication technologies electric consumption could explode in the following years. In 2012, networks, PCs, and data centers accounted for 4.7 % of the worldwide electric consumption [3]. In the worst-case scenario, this consumption could jump to 50 % by 2030 [4]. Rethinking the way electronic devices work to reduce their energetic costs and therefore their footprint is necessary. A promising solution to meet this tremendous challenge is the use of ferroelectric materials.

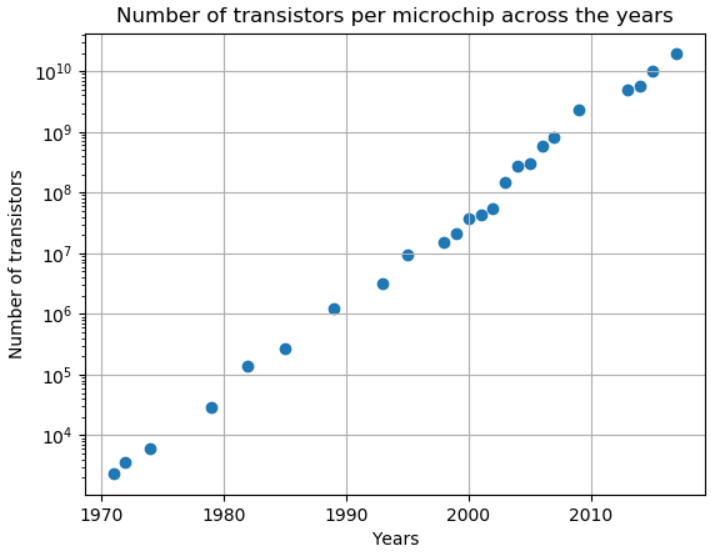

Figure 1.1: Illustration of the Moore's law, the number of transistors carried by a microchip is doubled every two years.

Ferroelectricity is a property of certain materials that possess a spontaneous polarization reversible by the application of an electric field. This feature leads to many industrial applications. They can be used as basic electronic element in non-volatile memory thanks to their ability to retain information or in capacitors where their high dielectric constant make them attractive. Because ferroelectrics are also pyroelectrics and piezoelectrics, they can be used in thermal infrared detectors, sensors or actuators [5]. Another appealing aspect of ferroelectricity is the possibility to couple it with ferroelasticity or ferromagnetism. This gives rise to a lot of potential applications where the benefits of both effects are exploited. For instance, multiple-state memory elements using both electric and magnetic polarization, *i.e.* the magnetoelectric coupling, have a huge potential in data storage technology [6]. This effect is also the pedestal of the magnetoelectric spin orbit (MESO) devices, a technology that could outshine the current technology in use in most electronics, the complementary metal-oxide semiconductors (CMOS) transistor [7].

The development of new ferroelectric materials requires a deepest understanding of their fundamental properties. The study of the mechanisms inducing ferroelectricity is therefore important. During the past decades, a lot of attention was given to perovskite ferroelectrics such as $BaTiO_3$, $PbZrO_3$ or $KNbO_3$. Their simple structures allowed the progression of phenomenological and first-principle models [8]. In this sense, they can be considered as a playground on which material scientists and physicists have built the methodology and the tools needed to their study. Nonetheless,

there is a need to extend our knowledge and our understanding to materials that have different structures, different chemistry and thus, different properties. In this master thesis, we will study Ba_4Sb_2O, a promising ferroelectric candidate recently discovered by our lab. We will try to understand what is inducing ferroelectricity using the tools that have been widely used for perovskite ferroelectrics.

Chapter 2

Essential concepts

We have just seen that ferroelectric can be combined with ferromagnetism to create magnetoelectric material exhibiting both properties. In fact, these two fields are very close because they share several common features such as a spontaneous polarization, presence of domains, hysteresis loop or the decrease in the magnitude of the polarization when increasing the temperature until a paraelectric or paramagnetic phase is reached. Actually, even the suffix ferro of ferroelectric originates from these numerous analogies and has nothing to do with the presence of iron [8]. First, a small reminder about ferromagnetism and its origin will be given. Then, we will present what is ferroelectricity, its definition, its connection with the dipole moment and the modern theory of polarization.

2.1 What is ferromagnetism?

Ferromagnetism is caused by a non-zero angular moment of the electrons which can be split into two terms, the orbital momentum which originates from the rotation around the nucleus and the spin momentum which is an intrinsic property of the electrons.

Consider a free atom with its electron shell filled. That means that every atomic orbital is occupied by two electrons. and according to the Pauli principle, one has it spin up and the other has its spin down. The sum of all the spin momentum **S** is thus zero. In the same time, each orbital with an orbital angular momentum bigger than one has an opposite counterpart resulting in a global orbital momentum **L** also equals to zero, resulting in a non-magnetic atom. However, when an electron from

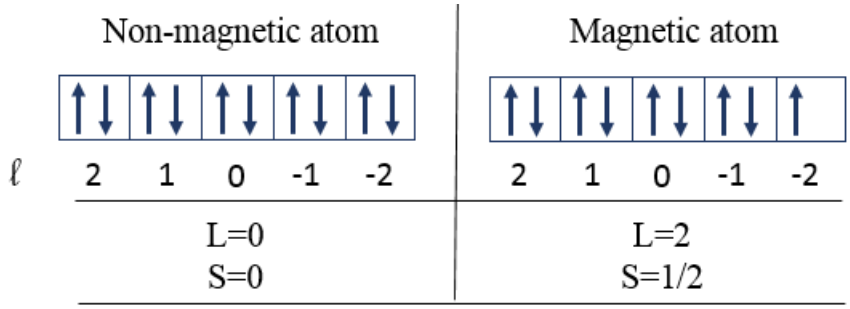

Figure 2.1: In the left panel, we see that an electron with a filled shell has both its spin momentum **S** and orbital momentum **L** equal to zero because each contribution is cancelled by an opposite equivalent. In the right panel, the withdrawal of a spin down electron in the l=-2 orbital leads to a non-zero angular moment since the spin up electron in the l=2 orbital has no opposite counterpart.

the shell is removed, all these statements are no longer true and the atom will have a net angular momentum and a magnetic moment (Fig 2.1).

In molecules, atomic orbitals are replaced by molecular orbitals but the reasoning stays valid. For instance, in the diamagnetic N_2, all the molecular orbitals are filled with two electrons and the global spin moment is therefore zero. In the other hand, in the paramagnetic O_2, two electrons with the same spin occupy two energetically equal molecular orbitals simply to reduce their coulombic interaction: if they had to share the same orbital, it would lead to a larger spatial overlap and the total energy of the system would be higher. This driving force is called the quantum exchange energy [8].

In solids the situation is slightly more complicated because electrons are often delocalized, orbitals let their place to electronic bands. Yet, the competition between exchange and coulombic energy is still present. In the ferromagnetic transition metals, Fe , Ni and Co, the $4s$ and the $3d$ bands are both located around the Fermi level but exhibit a different behavior. The former is broad and can only be occupied by 2 electrons resulting in a very low $states/eV$ whereas the latter, narrower and with a maximum occupation number of 10 has a high $states/eV$. Therefore, the exchange interaction in the $3d$ states is much more important and it results in the splitting of the up- and down-spin band, one having an higher occupation number than the other.

There is a further complication arising from the solid state. Even if all the conditions needed to have a magnetic moment are fulfilled, the solid is not necessarily magnetic at the macroscopic scale because of the presence of domains. A domain is a region where all the magnetic dipoles are oriented in the same direction and this in order to

reduce the total energy of the system [9]. A large domain is associated with a large magnetostatic energy which can be reduced by the splitting into smaller parts (Fig 2.2). This has a cost since the domain walls, the boundary between two domains, are highly frustrated in term of exchange energy.

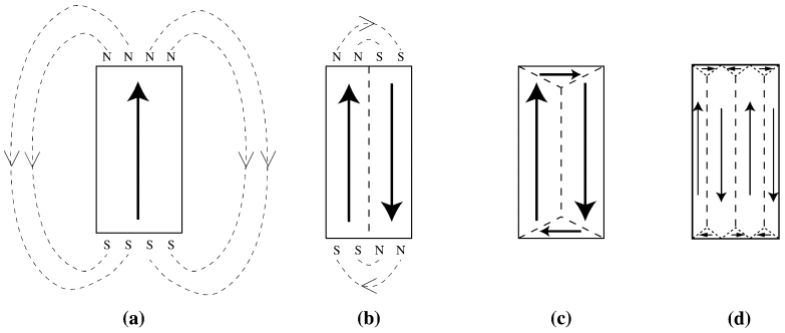

Figure 2.2: The subdivision of one large domain into smaller and smaller part will reduce the magnetostatic energy. Copied from [8].

An important aspect of ferromagnetism is the Curie temperature T_c. It is defined as the temperature at which a transition from the ferroelectric to the paramagnetic state occurs. When the temperature increases, the balance between the interaction energy of the magnetic dipoles J and the thermal energy $k_B T$ is being displaced towards the thermal energy which favors a random alignment of the magnetic dipoles. At T_c, the thermal energy becomes sufficiently high and all the magnetic contribution are cancelling each other. It results in a zero net magnetization and the sample becomes paramagnetic.

Anti-ferromagnetism is associated to an ordered magnetism with an important interaction energy between the magnetic dipoles. But unlike ferromagnetism, the dipoles are oriented in opposite directions. The result is that the net macroscopic magnetization is zero. As for ferromagnetism, there is a temperature, the Neel temperature, T_N at which the thermal energy becomes more important than the interaction energy. This means that an anti-ferromagnetic material heated above T_N will undergo a phase transition from anti-ferromagnetism to paramagnetism.

Another important feature is that the magnetization of a ferromagnetic material can be switched by the application of a sufficiently large magnetic field. The plot of these two quantities is called a hysteresis loop (Fig 2.3). This behavior can be understood by simple arguments. (1) Starting at origin and at $T < T_c$, the application of a magnetic field will orient the magnetic domains, initially oriented in random directions ($\mathbf{M} = 0$). The global magnetization will thus increase until it reaches its maximum value at the saturation field, meaning that all the domains

are aligned. The magnetic field is then decreased until it reaches zero (3), time at which the sample has a remnant magnetization (M_r). Afterwards, it is reversed and the magnetization reaches zero (4) when half of the domains are oriented in one direction while the other half is in the opposite direction. This point corresponds to the coercive field. By increasing the intensity of the field, one eventually arrives at another maximum value of magnetization (- M_s) where all the domains are again oriented in the same direction (5). To finish the loop, one has simply to cancel the total magnetization by the application of a coercive field in the other direction (6).

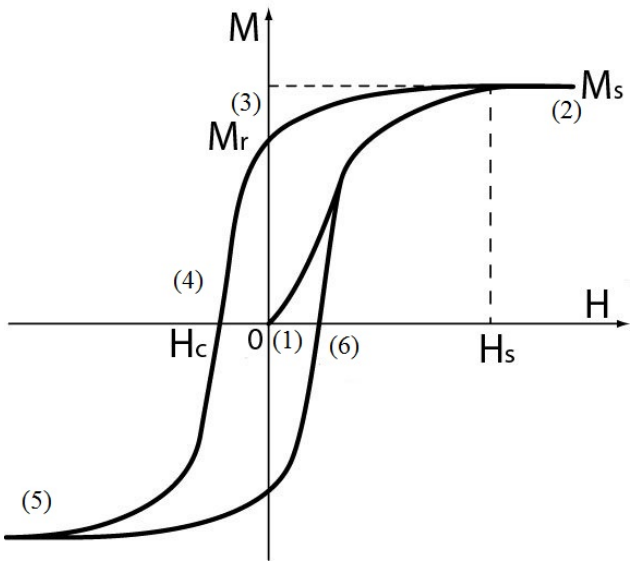

Figure 2.3: The measurement of the magnetization of a ferromagnetic sample as a function of the applied magnetic field leads to hysteresis loop, an important feature of this class of material. Copied from [10].

2.2 What is ferroelectricity?

Ferroelectricity was initially discovered in Rochelle salt in 1921 by the measurement of a hysteresis loop [11]. A few years later, the same behavior was found in K_2HPO_4 [12]. At first, these anomalies were thought to be associated to H because both compounds are characterized by H bonds but a decade later, ferroelectricity was also reported in $BaTiO_3$, a typical perovskite structure that does not contain H. Nowadays, the common definition of a ferroelectric is '*an insulating material that has at least two stable states with non-zero electric polarization switchable by the application of an electric field*' [8]. These two stable states usually originate from a symmetric structure which is spontaneously distorted. The signature of ferroelectric

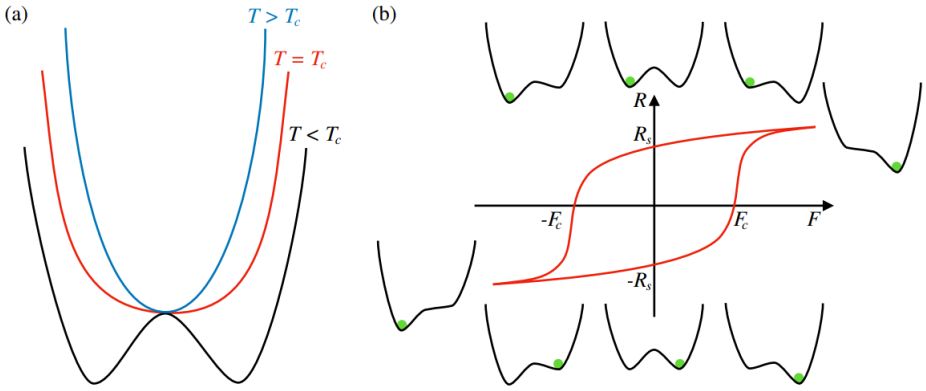

Figure 2.4: (a) At a temperature higher than T_c, the free energy curve is characterized by a single minimum, the symmetric state, but when T is decreased below T_c, two wells are formed which corresponds to the two stable ferroelectric state of opposite polarization. (b) Link between the hysteresis loop and the free energy curve. F is the force applied on the sample (the electric field for a ferroelectric) and R is its response (the electric polarization for a ferroelectric). The switching from one state to the other is triggered by the application of an electric field. Copied from [13].

can be found in the free energy curve with the formation of a double-well as shown in Fig 2.4. As for ferromagnetism, when the temperature is increased above the Curie temperature T_c, a phase transition from the ferroelectric to the paraelectric state occurs.

2.2.1 From molecular dipoles to macroscopic polarization

A molecule is said to be polar when it possesses an electric dipole, *i.e.* when one site has a positive charge and the other as a negative charge. Since this significantly impacts the various physico-chemical properties of chemicals such as solubility, reactivity, boiling point, etc. It is important to know whether a molecule is polar or not. In this case, the calculation of the total dipole moment $\mathbf{d}$ is straightforward and is given by the equation 2.1:

$$\mathbf{d} = \sum_i q_i \mathbf{r_i} \tag{2.1}$$

Where q_i are point charges and $\mathbf{r_i}$ are the positions. However, when a real piece of material is considered, the very large number of atoms ($\approx 10^{22}/g$) prevents the use of this formula. In the solid state, physical properties such as magnetization are usually expressed by volume unit and the natural choice in crystal is the unit cell volume. For the polarization $\mathbf{P}$, this leads to:

Figure 2.5: Infinite one-dimensional chain of alternated monovalent cations and anions. In this very simple idealized structure, the choice of unit cell leads to two different values of polarization.

$$\mathbf{P} = \frac{1}{\Omega}\sum_i q_i \mathbf{r}_i \tag{2.2}$$

Where Ω is the unit cell volume. One has then simply to calculate the dipole moment associated to one unit cell and to sum all these tiny contributions to find the macroscopic polarization. However, this approach known as the Clausius-Mossoti model is limited to purely ionic or molecular solids and is inadequate for compounds where a mix between covalency and ionicity exist. Another way to see that there is a conceptual problem within this approach is simply by considering the choice of unit cell.

Imagine an infinite uni-dimensional chain made up of an alternation of monovalent cations and anions with a regular interatomic distance (Fig 2.5). Intuitively, since each ion sits on an inversion center, the structure has no net **P**. However, the Clausius-Mossoti approach gives a different result because each unit cell has a dipole moment and worst, depending on the choice of unit cell you make, you would obtain two opposite values for **P**: $-\frac{1}{2}$ and $\frac{1}{2}$ [14].

The solution was to understand that the absolute value of **P** is ill-defined and the quantity of interest is change in polarization. In a practical experiment, the ferroelectric is used as a capacitor and the measurement of the current **j**(t) over time (equation 2.3) leads to a hysteresis loop (Fig 2.6) which can then be used to obtain **P** and **-P**. Then, the spontaneous polarization is simply half the difference between these two values. The key idea is that **P** is never directly measured but instead, it is Δ **P** which is obtain through the experiment.

$$\Delta\mathbf{P} = \int_0^t \mathbf{j}(t)dt = \mathbf{P}(\Delta t) - \mathbf{P}(0) \tag{2.3}$$

Going back to our 1D chain, what happened to our chain upon dimerization by the slight displacement d of the anions towards the cations (Fig 2.7), this can be

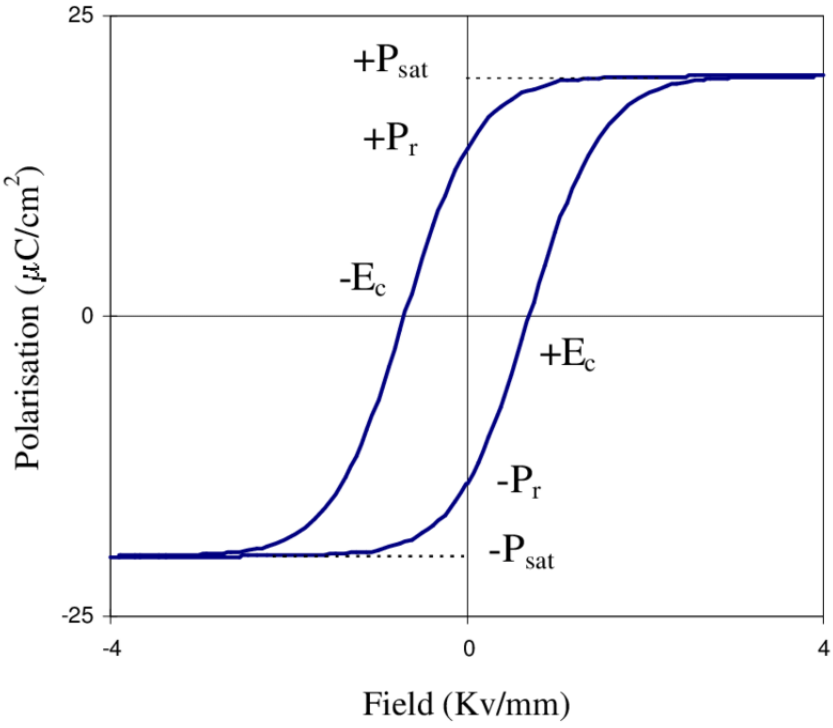

Figure 2.6: The measurement of **P** as a function of the electric field ϵ gives a hysteresis loop which can be used to obtain a precise value of the spontaneous polarization. P_{sat} is the maximum polarization the material can achieve and E_c is the coercive field, the electric field needed to reverse **P**. Copied from [15]

.

caused by a Peierls distortion. In the left unit cell, using eq. 2.2, we obtain a value of $-\frac{1}{2} - \frac{d}{a}$ and at right, we obtain $\frac{1}{2} - \frac{d}{a}$ and the difference in $\mathbf{P}$ between the centrosymmetric chain of Fig 2.5 and the polar chain of Fig 2.7 gives the same results: $-\frac{d}{a}$. This example of a 1D idealized chain which undergoes a Peierls distortion might seem artificial but there are situations where these concepts have been successfully applied to the design of new ferroelectric materials, especially in the field of organic ferroelectrics [16].

Figure 2.7: Dimerization of the 1D idealized chain which can be induced by a Peierls distortion for instance. The anions are shifted by a distance d to the left.

2.2.2 Antiferroelectricity

By analogy with antiferromagnetism, an antiferroelectric structure can be seen as an arrangement of electric dipoles oriented in opposite directions. Thus, they do not possess any spontaneous electric polarization at zero applied electric field. More generally, a material that has a phase transition between two non-polar state associated to a high dielectric permittivity can also be considered as an antiferroelectric [17]. They are characterized by a double hysteresis loop as shown in Fig 2.8.

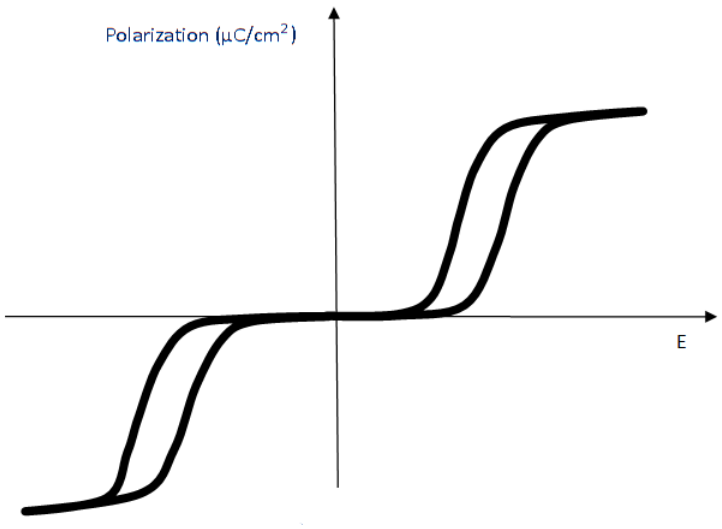

Figure 2.8: Hysteresis loop of an antiferroelectric material. Modified from [18]

The most common antiferroelectric is probably $PbZrO3$, another perovskite. Some of their applications include high-energy electric supercapacitors, electrocaloric refrigerators or transducers [19].

2.2.3 Domains

We have briefly discussed the existence of domains in the section about ferromagnetism where their role is to diminish the global energy of the system. For similar reasons, ferroelectric materials are also characterized by their presence. So far, we have mainly discussed about bulk polarization without any considerations about the effects at the boundaries of the solid. The polarization generates a surface charge density defined as $\sigma = \mathbf{P}\hat{n}$ where $\hat{n}$ is a vector perpendicular to the surface. This produces an electric field inside and outside the material which tends to cancel the spontaneous polarization of the ferroelectric and is hence called the depolarization field.

Like a capacitor where the energy stored in the electric field depends on the electric charges at the conductive plates, the higher the surface charge density, the higher the field and the higher the energy stored in it. A ferroelectric will have a natural tendency to diminish the surface perpendicular to the direction of the polarization. For this reason, the polarization in a thin film ferroelectric is directed along the plane rather than perpendicular to it to decrease the surface charge density [8]. In bulk ferroelectrics, polarization tends to be parallel to the surface and this can only be achieved by the presence of domains (Fig 2.9). Contrary to ferromagnets where the domain wall energy is governed by the exchange energy, ferroelectric domain walls are mainly dominated by the polarization energy and its coupling with the strain. Since the interaction energies are more important in this case, the change of direction of the polarization occurs on a shorter length scale, usually of the order of a few unit cell [20].

2.2.4 Born effective charges

Quantities of particular interest in ferroelectricity are the Born effective charges. These tensors express the variation of the polarization $\mathbf{P}$ in the α direction with the atomic displacements r of the atom i in the β direction. Ω is the unit cell volume:

$$Z^*_{i,\alpha\beta} = \Omega \frac{\partial P_\alpha}{\partial r_{i,\beta}} \tag{2.4}$$

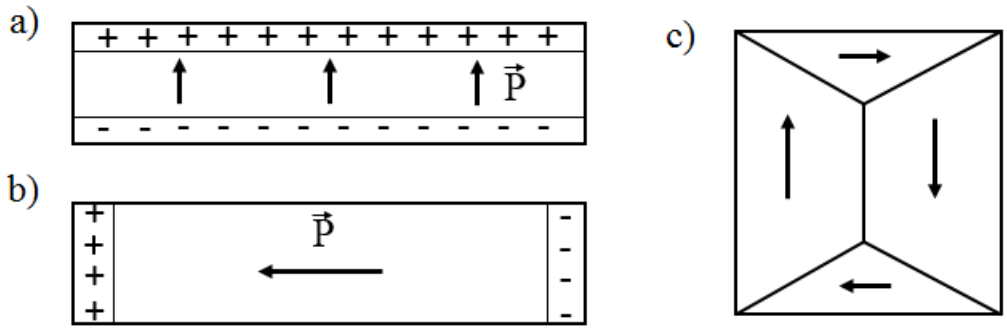

Figure 2.9: (a) A polarization perpendicular to the plane of the film leads to a high surface charge density and consequently, to an important energy associated to the depolarization field. (b) The energy cost can be reduced simply by reorienting the polarization in the direction of the plane. (c) In a bulk ferroelectric, domains are necessary to ensure that the polarization is always parallel to the surface.

A consequence is that an ion with a large Born effective charge will generate a large dipole moment even for small displacement. The term anomalous Born effective charges refers to the effect where the Born effective charges are larger than the nominal ionic charges. It is commonly found in ferroelectric perovskites and will be discussed more deeply in the result section. By analogy with the concept of electric charge, they are also defined as the force **F** induced on the ion by an electric field ϵ:

$$Z^*_{i,\alpha\beta} = e\frac{\partial F_{i,\alpha}}{\partial \epsilon_{i,\beta}} \tag{2.5}$$

Where e is the elementary charge. Interestingly, if one has access to the Born effective charges and the atomic displacements of the corresponding ions, it is possible to calculate **P** by rearranging equation 2.4. However, Born effective charges are sensitive to structural deformations, especially when they involved changes in the electronic structure [21] and an integration over the displacement should be realized instead. In the next section, a more formal way to calculate **P** is presented.

2.2.5 The modern theory of polarization

Most of the concepts that have been formulated previously take their roots in the modern theory of polarization which is also known as the Berry phase approach. The goal of this section is to give the reader a more robust formalism of the physics behind the theory. To keep things simple, only the main results will be presented.

At the basis of this theory stands the idea that $\mathbf{P}$ can only be measured through the macroscopic current density (equation 2.3). At $t = 0$, we suppose that our system is in a centrosymmetric state and we express all the sublattice displacements through a variable λ that varies from 0 (centrosymmetric state) to 1 (ferroelectric state):

$$\Delta\mathbf{P} = \int_0^1 \frac{d\mathbf{P}}{d\lambda} d\lambda \tag{2.6}$$

Assuming the Born-Oppenheimer approximation, we can decompose the ionic contribution and the electronic contribution:

$$\Delta\mathbf{P} = \Delta\mathbf{P}_{ions} + \Delta\mathbf{P}_{el} \tag{2.7}$$

And considering ions as point charge, we can simply use 2.2 to find the associated polarization. The derivation of the electronic contribution was realized by King-Smith and Vanderbilt [22] but will not be detailed here. The final result is expressed as a Berry phase, hence the name of Berry phase approach.

$$\mathbf{P}_{el}(\lambda) = \frac{ei}{(2\pi)^3} \sum_n \int_{BZ} \langle u_{n\mathbf{k}} | \nabla_{\mathbf{k}} | u_{n\mathbf{k}} \rangle d\mathbf{k} \tag{2.8}$$

The sum runs over all occupied band and the integral is over the first Brillouin zone. The $u_{n\mathbf{k}}$ are the eigenfunctions of the Schrödinger equation, assuming periodic boundary conditions and the use of the Bloch theorem $\psi_{n\mathbf{k}}(\mathbf{r}) = e^{i\mathbf{kr}} u_{n\mathbf{k}}$.

Because of the periodic boundary conditions, $\mathbf{P}$ is a multi-valued quantity as we have seen in the case of the 1D chain where $\mathbf{P}$ was $-\frac{1}{2}$ or $\frac{1}{2}$. Depending on the choice of unit cell you make, you could also obtain $-\frac{3}{2}$, $-\frac{5}{2}$ or $\frac{7}{2}$ and all the values that $\mathbf{P}$ can take is called the polarization lattice. Actually, the fact that it is centrosymmetric around zero is the signature of a paraelectric structure. The difference between two consecutive values is the quantum of polarization, in this case 1. More generally, the quantum of polarization is equal to $e\mathbf{R}/\Omega$ with $\mathbf{R}$, a lattice vector.

2.3 Magnetoelectric materials

We just saw in details what are ferromagnetism and ferroelectricity. To avoid confusion, a small word about the taxonomy of all the concepts linked to ferroelectricity

seems necessary for the sake of clarity. Ferroics is a class of material that exhibits large changes of a physical property in a narrow range of temperature. They are characterized by hysteresis loops and by the existence of two distinct states switchable by the application of the correct perturbation. Ferromagnets and ferroelectrics are part of this family since their polarization - electric or magnetic - can be reversed by the application of an external - electric or magnetic - field. Another member of ferroics are ferroelastic materials in which the application of a pressure results in a spontaneous strain and is considered as the mechanical analogue of the two others. The relationship between them is illustrated in Fig 2.10.

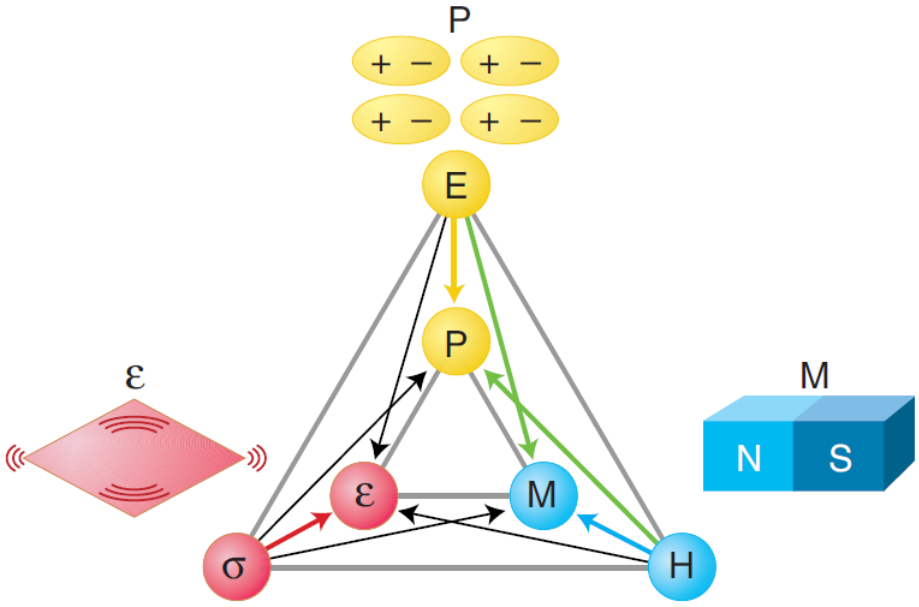

Figure 2.10: Relationship between the electric field E and the polarization P, the magnetic field H and the magnetization M, the stress σ and the strain ϵ. Copied from [6]

.

A material subject to at least two distinct ferroic properties is called multiferroic. The combination of ferroelectricity and ferromagnetism, the magnetoelectric multiferroicity [6], is of great interest not only because of the presence of the two functionalities at the same time but also because these materials are subject to the magnetoelectric coupling. Furthermore, it is difficult to access to large values of magnetic fields for practical purposes. This provides a way to obtain large magnetic answer by applying large electric field, easier to obtain and to control. The magnetoelectric coupling brings the possibility to control magnetic properties with an electric field and reversely, to control electric properties with a magnetic field. The expansion of the free energy G can highlight the presence of this coupling [8], for simplicity we consider that the temperature and pressure are constant:

$$G(E,H) = G_0 + P_i E_i + M_i H_i + \frac{1}{2}\epsilon_{ij} E_i E_j + \frac{1}{2}\mu_{ij} H_i H_j + \alpha_{ij} E_i H_j + \frac{1}{2}\beta_{ijk} E_i H_j H_k + \frac{1}{2}\gamma_{ijk} H_i E_j E_k + ... \quad (2.9)$$

Where ϵ_{ij}, μ_{ij} are the electric and magnetic permittivity in direction i, j. α_{ij} is the linear magnetoelectric susceptibility tensor and β_{ijk}, γ_{ijk} are the bilinear magnetoelectric susceptibility tensors. There is a fundamental difficulty to combine both effects in the same phase: ferroelectrics must be insulators while most of the elemental ferromagnets such as Fe or Co are metallic. Worst, as we have seen in section 2.1, it is even a requirement since it is the high density of levels around the Fermi level that drives the magnetic behavior.

Another complication arises from the study of ferroelectric perovskites $ABO3$, one of the most studied ferroelectric family. Hill showed in 2000 that the combination of both effects in the same phase is difficult because of electronic configuration requirements [23]. We will see in the case study of $BaTiO3$ that the ferroelectricity is triggered by the movement of the metallic atom Ti because it has an empty electron shell. However, this hindered the presence of magnetism since it requires partially filled d orbitals. Fortunately, despite the d^0 criterion plays a crucial role in the ferroelectric behavior of several structures such as $KNbO3$ or $PbTiO3$, there are other route towards ferroelectricity. A solution is to make a distinction between the atoms that will induce ferroelectricity and ferromagnetism. In the promising multiferroic $BiFeO3$, the off-center displacement is driven by the stereochemical activity of the s lone pair of Bi while the d^5 electronic configuration of Fe brings the magnetic behavior [24]. Conversely, in $EuTiO3$, it is the Eu^{2+} in the A-site that generates a non-zero magnetic moment but its small size hampers the Ti movement and ferroelectricity is only reached under strain [25].

To be used in everyday life applications, multiferroic materials have to fulfill one specific requirement. That is a sufficiently high Curie temperature or Neel temperature, at least close to the room temperature. However, over the several families that have been investigated, only $BiFeO3$ had a Curie and Neel temperature higher than the room temperature in 2011 [26]. Since then, new materials with high Curie temperature have been discovered such as $(PbFe_{0.5}Nb_{0.5}O3)_x(PbZr_{0.5}Ti_{0.47}O3)_{(1-x)}$ [27].

Chapter 3

Applications

3.1 Ferroelectric Random-Access Memory

Computers roughly use two main types of memory; the storage memory where the files, folder, papers, movies, etc. are stocked is characterized by a long access time, a cheap cost and by its non-volatility. Volatility is an important feature of memory which defines whether your data are kept when the power supply is turned off. A non-volatile memory keeps the data intact whereas a volatile memory loses every information.

Besides the storage memory, there is the random-access memory (RAM): it is fast, expensive and volatile. There is a further distinction between static RAM and dynamic RAM (DRAM). In the latter, the memory cells are usually made up of a transistor and a capacitor that stores the data by being charged or discharged. The problem is that there is a leaking current associated to the capacitor when it is charged meaning that the information has to be constantly refreshed, typically every 64ns [28]. Hence, the name of dynamic RAM. This has also an important impact on the energy consumption of the electric devices.

By contrast, ferroelectric random-access memory (FeRAM) exhibits several advantages such as a low power consumption, fast read-write operations and a high endurance (10^{13} cycles) [29], making it a potential successor to the current DRAM technology. FeRAM memory cells use polarization to store information. In ferroelectrics, the ground state possesses a non-zero polarization value even without electric field. Thus, the data is retained when the power supply is cut-off making the technology non-volatile.

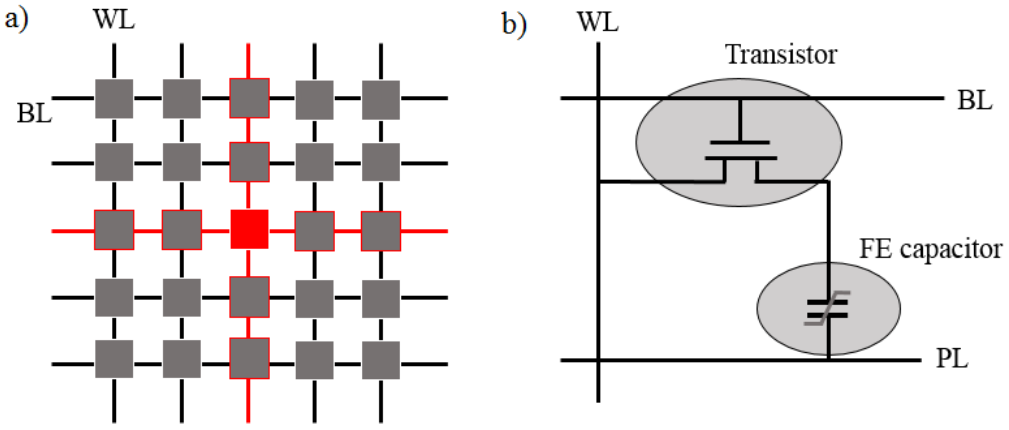

Figure 3.1: (a) In the cross-point architecture, the memory cells are placed on a grid and to ensure the selectivity, only half the voltage needed to switch the polarization is applied in the bit (BL) and the world (HL) lines. Thus, only the one at the crossing of the activated lines (in red) get a sufficient voltage to be switched. (b) In the 1T-1C configuration, to avoid the crosstalk problem associated with crosspoint architecture, a transistor is added to each cell to control whether the current should pass or not into the ferroelectric capacitor.

In the early stage technology, the memory cells were arranged in order to form a grid joined by horizontal (bit lines) and vertical wires (word lines), as shown in fig 3.1 (a). The writing operation, *i.e.* the switching of the polarization inside a cell to rewrite information, was done by applying half the voltage required along the bit line and the other half along the word line. Thus, the neighbors of the cell were not affected by its switching. However, the application of half the required voltage could sometimes be sufficient to reverse the polarization of neighboring bits meaning that information could be destroyed against our will [8].

To avoid the crosstalk problems, the solution is to use a configuration consisting of a transistor and a 1 ferroelectric capacitor (fig 3.1 b). The transistor now isolates the capacitor from the other cells. The information is written by applying a voltage superior to the coercive field that will reorient the dipoles of the ferroelectric in the corresponding direction. In the reading operation, a voltage is also applied to the cell and the current is measured. If the dipoles are oriented in the direction of the electric field, then the measured current is the one associated to the charging current of the capacitor. Otherwise, the measured current is higher since there is a switching current due to the reorientation of the dipoles in addition to the charging current of the capacitor [30].

This technology reached its apogee in 2003 when it was used in the Sony PlayStation 2 game console [31]. However, to further miniaturize FeRAM, the passage from a

2D planar to a 3D high density capacitor structure became necessary. This effort was hampered by the scarcity of 3D perovskite-based capacitors - only two were considered, $PbZr_xTi_{(1-x)}O_3$ and $SrBi_2Ta_2O_9$ [32]. Recently, the discovery of ferroelectricity in Si-doped HfO_2 has revived the interest for FeRAM as it provides a promising route to pursue its miniaturization [33].

3.2 Negative capacitance

Before explaining what is negative capacitance and how is it related to ferroelectrics, let's start by a quick reminder on field effect transistors (FET). One of the main challenges in the field of electronics is to shrink more and more the components of integrated circuits to increase their compactness. This is what the Moore's law of Chap 1 is about.

Illustrated in the left panel of Fig 3.2, a FET is a basic component used in most of our electronic devices. It contains three distinct layers. The bottom one is divided in three parts: the channel is an intrinsic semi-conductor while the source and the drain are n- or p-doped semi-conductor and are linked together by electrodes. The electronic properties of this region are controlled by the gate, a semi-conductor control electrode which acts as a switch. When a voltage V_g is applied, it generates a depletion zone in the channel that allows the current to pass from the source to the drain. The separation between the gate and the bottom layer is realized with an insulating layer.

The right panel of Fig 3.2 shows the electric circuit analogue of the FET. It can be seen as two capacitors in series; the first is associated to the gate-insulator-channel part and has a capacitance C_{ins}. The second corresponds to the source-channel-drain region and has a capacitance C_s. The in-between voltage is ψ_s

There are two fundamental limits to how much a FET can be shrunk. First, the tunneling current from the source to the drain increases as the size of the channel is decreasing. The other complication is more subtle and is commonly known as the Boltzmann Tyranny. The channel can be seen as a barrier that electrons have to overcome to pass from the source to the drain. We just saw that the height of the barrier could be decreased by the application of a voltage across the gate. The electron distribution obeys a Boltzmann distribution, thus the current to pass under the application of a voltage is $exp(\frac{eV_g}{k_bT})$. From this, we see that the minimum voltage to increase the current by an order of magnitude is 60 mV at room temperature [34]. The Boltzmann Tyranny refers to this value since it limits the minimal size of a

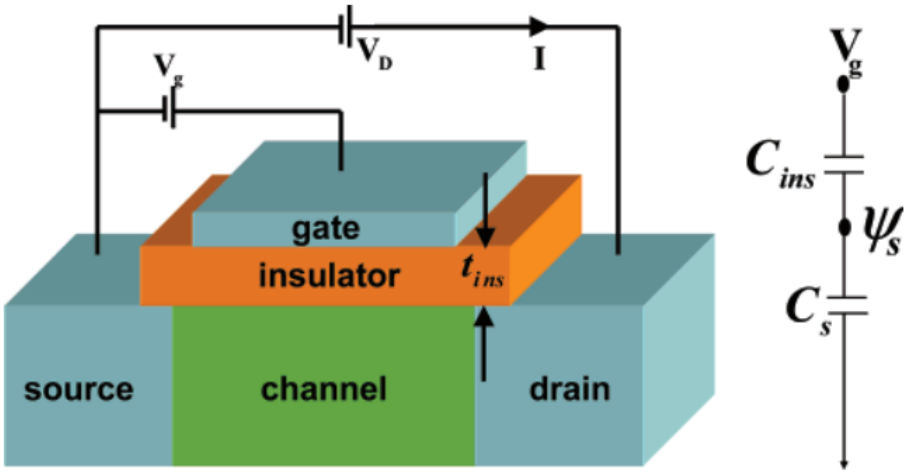

Figure 3.2: Structure of a FET. The electron flux moving from the source to the drain is blocked at the channel, a semi-conductor. But the application of a sufficient voltage V_g will decrease the energy barrier and let the current pass. On the left, the equivalent electric circuit made up of two capacitors, C_{ins} is the insulator capacitance and C_s the the semi-conductor capacitance. Copied from [35].

transistor. Indeed, the higher the energy needed to switch, the higher the associated energy loss which heat the surrounding and eventually lead to the breakdown of the device.

Negative capacitance can provide a way to supplant the Boltzmann Tyranny [35]. To highlight that, we write this requirement as:

$$S \equiv \frac{\partial V_g}{\partial(log_{10} I)} = \frac{\partial V_g}{\partial \psi_s} \frac{\partial \psi_s}{\partial(log_{10} I)} \tag{3.1}$$

Where S is the subthreshold swing value and ψ_s is the voltage between the two capacitors which can be related from electric circuit analysis to V_g:

$$\frac{\partial V_g}{\partial \psi_s} = 1 + \frac{C_s}{C_{ins}} \tag{3.2}$$

If C_s and C_{ins} are positive, we see that the minimal value $\frac{\partial V_g}{\partial \psi_s}$ can reached is 1. Thus, the only way to reduce S below 60 $mV/decade$ is to have a negative C_{ins}.

From basic electronic, we have that $dQ = \frac{dC}{dV}$ and $U = \frac{Q^2}{2C}$ where U is the potential energy stored in a capacitor. The plot of these relationships for a linear capacitor and a hypothetical negative capacitance is shown in Fig 3.3.

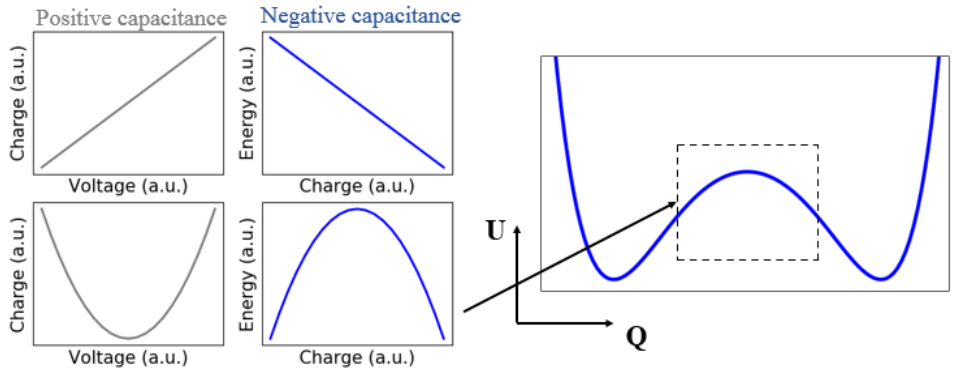

Figure 3.3: On the left, the plots of the charge against the voltage and of the potential energy against the charge for a positive and a negative capacitor. On the right, the similarity the free energy curve of a ferroelectric and its double-well signature.

The W-shaped form in Fig 3.3 resembles the free energy curve of a ferroelectric. A ferroelectric capacitor can be in two distinctive capacitance regimes depending on its state. While a positive capacitance should be expected around the two minima of the energetic landscape, a negative capacitance can be achieved close to the maximum. However, it unfortunately corresponds to the unstable symmetric structure meaning that negative capacitance cannot be measured as a time independent property. When a voltage is applied across a ferroelectric capacitor, the energetic landscape will be tilted until one of the two minima disappeared at the coercive field (Fig 3.4). After almost 10 years of experiments, a negative capacitance was demonstrated in $Pb(Zr_{0.2}Ti_{0.8})O_3$ with a small decrease of the voltage across the capacitor upon the application of a voltage pulse [36].

We have seen that negative capacitance is associated with the transition from the non-polar to the polar state. A uni-dimensional chain model made up of polarizable units was used to gain insights on the microscopic origin of ferroelectricity [37]. These units are inside an electric field E_{local} with two components, the applied electric field E_{app} and the electric field generated by the dipoles E_{dip}. Since E depends on E_{dip} and, the dipole moment of each units depends on E, there is a positive feedback mechanism that leads to a highly unstable situation. Indeed, at zero applied electric field, any thermal fluctuations of one dipole will immediately orientate the neighboring units. According to this model, when $T < T_c$, the polarizability - inversely proportionate to T - becomes sufficiently high to trigger the positive feedback mechanism. The local electric field is therefore amplified meaning that the dipoles can be oriented in the opposite to the applied electric field. It generates the macroscopic polarization and the negative capacitance.

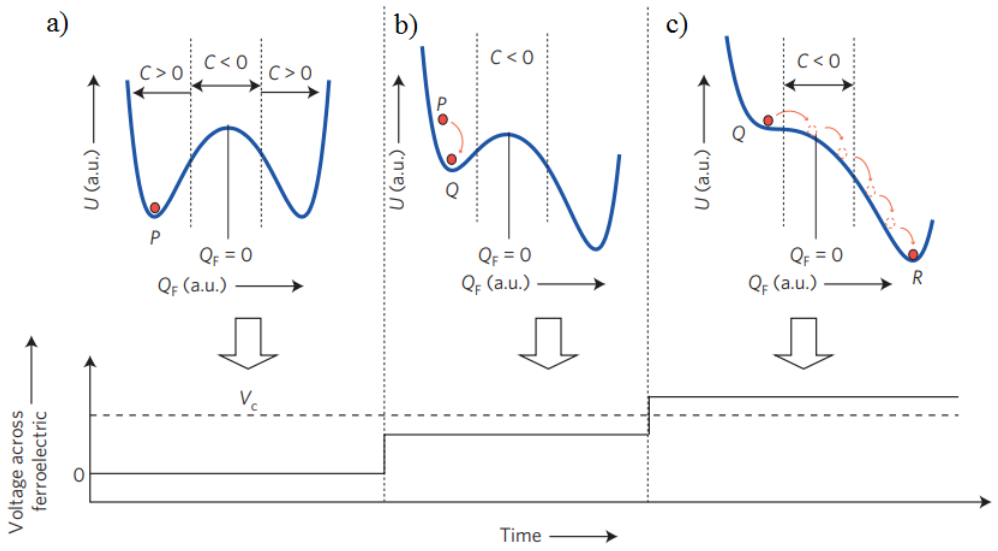

Figure 3.4: Energy landscape of a capacitor ferroelectric as a function of the charge accumulated under different voltage. (a) At zero applied voltage, the free energy curve shows its familiar a double-well potential with its corresponding capacitance regimes. (b) The application of a voltage smaller than the coercive voltage is not sufficient to switch the polarization and negative capacitance is not achievable yet. (c) Finally, when the voltage is higher than the coercive voltage, the free energy curve exhibits only one minimum and during the transition, the capacitor moves to a negative capacitance state. Copied from [36]

3.3 Magnetoelectric effect applications

One of the most interesting aspect of magnetoelectric materials is the possibility to control magnetic properties with an electric field and reversely. The first steps in this direction were achieved with the reorientation of antiferromagnetism by the application of an electric field in $BiFeO_3$ [38]. A decade later, the same material was combined with a ferromagnetic layer of a FeCo alloy in a thin-film to electrically switch the magnetization [39]. More interestingly, this research group manages to apply the effect to control an energy efficient spin-valve device, thereby opening the door to a lot of possible applications.

3.3.1 Magnetoelectric spin orbit (MESO) logic device

The field of electronics have been dominated by the complementary metal oxide semiconductors (CMOS) technology during the last decades. CMOS is a very general term that describes electronic components based on a metal, an oxide and a semiconductor. For instance, the FET of the previous section is an example of a CMOS device since it contains the three different elements. However, this technology is running out of steam especially in term of miniaturization and energy consumption has we just saw.

MESO logic devices is an emerging technology that could eventually outshine CMOS. Indeed, the energy required to the switching in a MESO logic device could be 30 times lower than in the most advanced CMOS device while working at a voltage 5 times lower and with a logical density that could be 5 times higher [7].

The operation scheme of a MESO logic device is shown in Fig 3.5. It consists of a magnetoelectric switching capacitor, a ferromagnet and a spin-to-charge conversion module. The idea is to use two transducers to pass from electricity to magnetism using the magnetoelectric material and then to go back from magnetism to electricity with a spin-orbit transducer. First, the electric current is converted by the magnetoelectric into a magnetic polarization in the ferromagnet. The readout is done by applying a supply current to this nanomagnet, this releases a flow of spin-polarized electrons in the spin-orbital coupling transducer which in turn generates the output current.

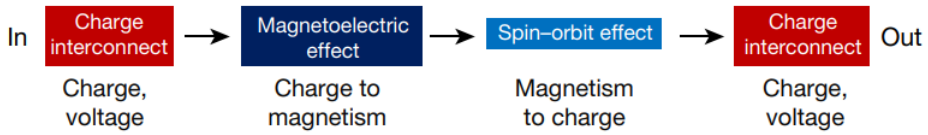

Figure 3.5: The operation scheme of a MESO logic device: first an electric current is transformed into a magnetic polarization using the magnetoelectric effect followed by the reverse operation during which the magnetization is converted back into an electric current using a spin-orbit transducer. Copied from [7]

3.3.2 Drug delivery particles

Ferromagnetic particles were proposed for biomedical applications in the 70's [40]. The idea is to avoid the general distribution of the drug through the body by using a magnetic field to guide ferromagnetic nanoparticles carrying the drug to a specific

target such as a tumor. The release of the content can be then triggered through an enzymatic activation or through physiological changes [41].

Multiferroic materials are a promising candidate to enhance this methodology. The advantage of using multiferroic instead of ferromagnetic particles is that the magnetic field can control the electric polarization of the capsule to change its surface charge. This induces the destruction of the shell around the drug and its delivery at the right place [42]. In this case, there is no need for specific biologic conditions. This technology could also be interesting for the medical treatments of cancer, AIDS or Parkinson's disease [43].

Chapter 4

Objectives

This works begins with an analysis of a well-known and widely studied material, $BaTiO_3$. The goal is to reproduce some known results and thereby to validate the tools and methods used subsequently. The analysis includes mainly Born effective charges, polarization and density of states (DOS) calculations.

During the second part, a study over A_4Sb_2O compounds, where A is an alkaline-earth will be realized. It focuses mainly on Ba_4Sb_2O: this material was recently identified by our laboratory as a promising ferroelectric candidate of this series. The properties of interest like the Born effective charges and the polarization amplitude will be calculated.

Investigations over the origin of the ferroelectric behavior using mainly DOS and COHP analysis and a comparison with $BaTiO_3$ will then be realized. The role of chemistry in this system will also be investigated by substituting Ba with two other alkaline-earth, Sr and Ca. Finally, we will study the behavior of Ba_4Sb_2O under strain.

Computational methods

All the calculations were performed using the Vienna Ab-Initio Simulation Package (VASP) [44], a DFT code using the projector-augmented-wave (PAW) method [45]. For $BaTiO_3$, the relaxation calculations were done using a (8x8x8) k-points mesh, a cutoff energy of 520 eV and the PBE exchange-correlation functional [46]. For the DOS calculations, a (20x20x20) k-points mesh was used, the other parameters were the same. For Ba_4Sb_2O, Sr_4Sb_2O and Ca_4Sb_2O, we used a (8x8x4) k-points mesh

((20x20x9) for the DOS calculations). Born effective charges were obtained using the density functional perturbation theory (DFPT) and with the same parameters than for the relaxation calculations. The COHP analysis [47] was realized on conventional cells with a (12x12x3) k-points mesh using the lobster package.

Chapter 5

$BaTiO_3$

Discovered in the middle of the 40's [48], $BaTiO_3$ was the first ferroelectric oxide to be identified. In its paraelectric phase, it corresponds to an ideal cubic perovskite structure of the chemical formula ABO_3 where A and B are divalent and tetravalent cations, respectively. As shown in Fig 5.1 a), the B cations are located at the center of an octahedron made up of O while the A cations are found on the edge of the cube constructed by this octahedron. The corresponding space group is $Pm\bar{3}m$.

Below the Curie temperature (393K), the structure undergoes a phase transition to a ferroelectric tetragonal phase ($P4mm$) in which the Ti atom is shifted along the c axis, *i.e.* in the [001] direction (Fig 5.1 b). The measured polarization has a value of 27 $\mu C/cm^2$ [8]. At 278K, another phase transition happens with a passage to an orthorhombic system ($Amm2$); this can be seen as an elongation of the cubic phase along the [011] direction (Fig 5.1 c). Finally, a last phase transition to a rhombohedral system ($R3m$) occurs at 183K, with the direction of the distortion being [111] (Fig 5.1 d). These two low temperature phases are also ferroelectric with polarization value of 36 $\mu C/cm^2$ and 33 $\mu C/cm^2$ for the orthorhombic and rhombohedral phases, respectively. At this point, it is important to mention that we will be mainly focusing on the cubic and the tetragonal phases. Indeed, most of the results that will be of significant importance for the analysis of A_4Sb_2O can already be found from these two.

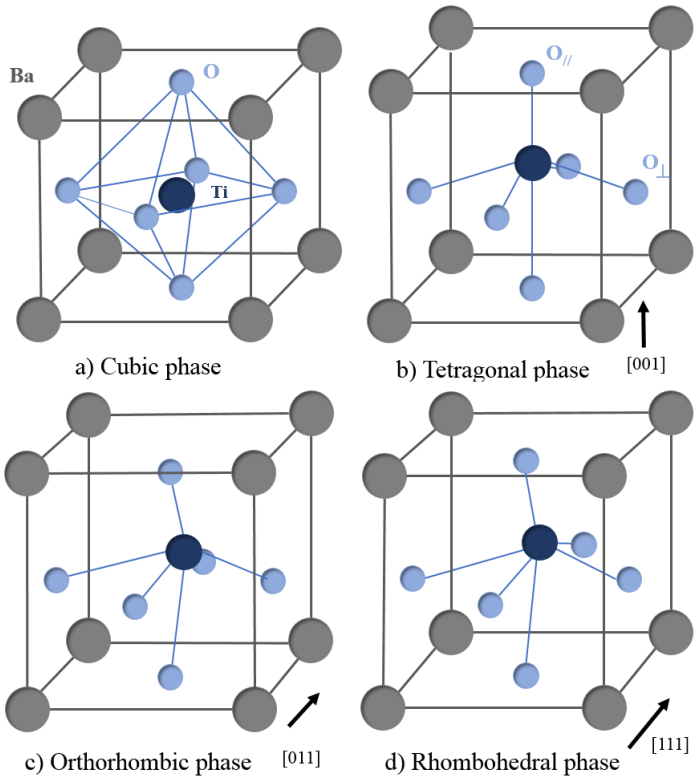

Figure 5.1: a) Cubic centrosymmetric structure of BaTiO3. At 393K, the system undergoes a transition towards a ferroelectric tetragonal (b) phase of BaTiO3. At 278K, another phase transition happens and BaTiO3 adopts an orthorhombic system (c). Finally, the last change occurs at 183K when a rhombohedral symmetry is obtained (d).

5.1 Ferroelectricity as a structural instability of unstable phonon modes

5.1.1 Phonons

In a diatomic molecule, only one vibrational mode exists which corresponds to the stretching of the bond. The vibration can simply be described by the distance between the two atoms. More generally, linear molecules possess 3N-5 vibrational modes and non-linear molecules 3N-6, N being the number of atoms. From quantum mechanics, there is a series of energy associated to each of these vibrational modes given by $E_v = \hbar\omega(n + \frac{1}{2})$ where ω is the frequency of the mode and n is a quantum number.

The description of the vibrational modes in a solid is more complicated because of the

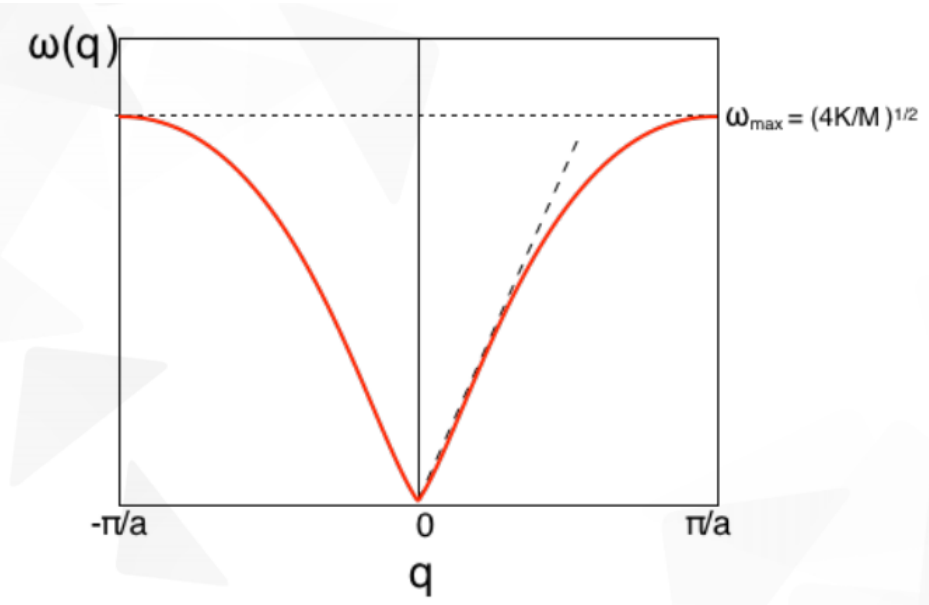

Figure 5.2: Phonon dispersion relation for an infinite linear uni-dimensional chain. Copied from [50].

large number of atoms but we can rely on the symmetry if the solid is crystalline. Starting from an infinite linear uni-dimensional chain made up of atoms bonded together by springs, one can retrieve the dispersion relation [49]:

$$\omega = 2\sqrt{\frac{C}{m}}|sin(\frac{qa}{2})| \tag{5.1}$$

Where ω is the frequency, C is the elastic constant of the spring, m is the mass of the atom, q is the wavenumber and a is the interatomic distance. The plot of ω as a function of q, the dispersion relation, is illustrated in Fig 5.2.

Only the values of q between $-\pi$ and π gives independent vibration modes. In the longitudinal modes, the atoms are moving around their equilibrium positions in the direction of the vibration while in the transverse modes, they are moving perpendicularly to the direction of vibration. These two distinct vibrational regimes are shown in Fig 5.3.

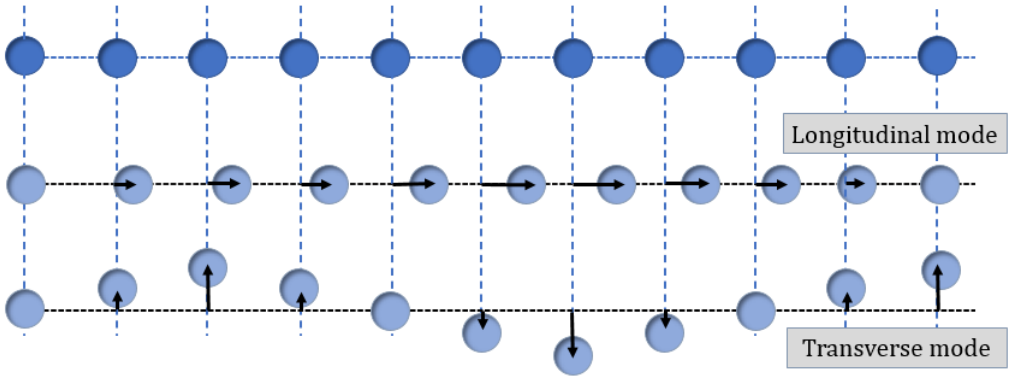

Figure 5.3: Longitudinal and transverse modes in a linear one-dimensional infinite chain.

When the structure is made up of two different atoms, the resolution of the equation associated to this system leads to two possible solutions. This means that there is now two bands instead of one as shown in Fig 5.4. If the solid is ionic or that the electronegativity difference between the two atoms is sufficiently large, the optic modes can be excited by an electromagnetic field, thus giving it the name optic. In crystals, the number of dimensions is 3 and the wavenumber becomes a wave vector $\mathbf{q}$ and the phonon dispersion relations is usually represented for a given path in the first Brillouin zone.

The quantum nature of an atomic system tells us that the energy is exchanged by quanta. In the case of vibration in solids, this quantum of vibration is called a phonon. The situation is similar to the electronic structure from molecules to solid. Molecular orbitals are used to describe the first while electronic bands relating the energy and the wave vectors are used in the latter.

5.1.2 Phonon instabilities

Numerous attempts have been made to understand the origin of the phase transitions in $BaTiO_3$. In 1960, Cochran proposed that ferroelectricity in $BaTiO_3$ could be related to the lattice dynamics and more precisely, to an instability of certain modes of vibration [51]. In this model, it is the softening of a transverse optic phonon mode caused by the temperature drop that leads to a ferroelectric instability. The presence of these soft-modes has been highlighted on $BaTiO_3$ by infra-red experiments [52] and ab-initio calculations [53] (Fig 5.5). We observe that negatives frequencies are found not only at Γ but also along the Γ-X, X-M and M-Γ paths. Focusing on the Γ point, the application of the dynamical equation (5.2) allows one to retrieve

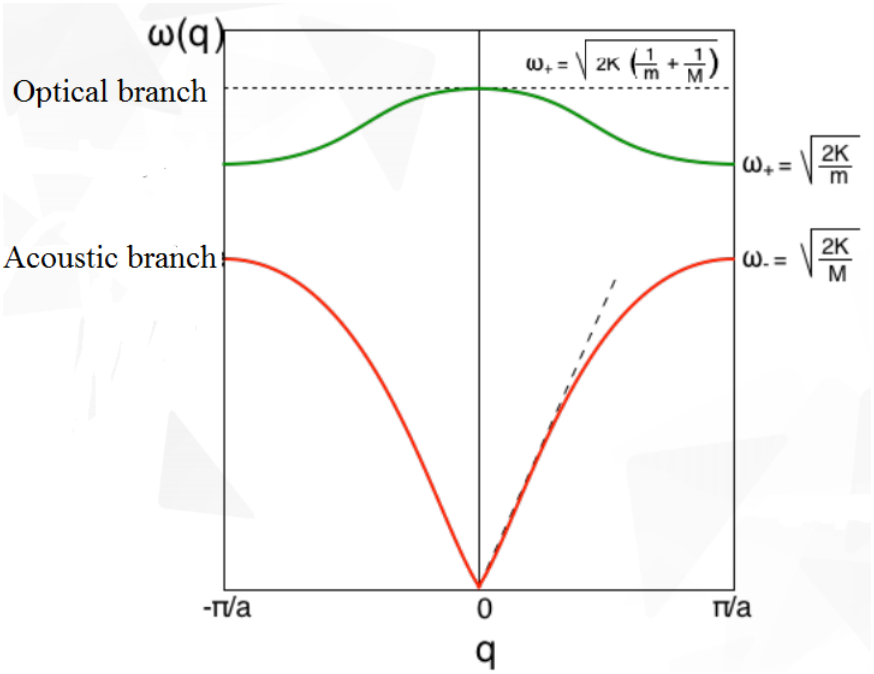

Figure 5.4: Phonon dispersion relations for an infinite linear chain made up of two different atoms. Two different branchs are visible, the acoustic branch and the optic branch. Modified from [50].

the associated atomic displacements (Fig 5.5 b) which actually corresponds to the deformation towards the tetragonal phase.

$$D_{\mathbf{q},j}\mathbf{e}_{\mathbf{q},j} = \omega^2_{\mathbf{q},j}\mathbf{e}_{\mathbf{q},j} \tag{5.2}$$

Where $D_{\mathbf{q},j}$ is the dynamical matrix, $\mathbf{e}_{\mathbf{q},j}$ are the eigenvectors and $\omega^2_{\mathbf{q},j}$ are the frequencies associated to the mode of vibration j at wave vector q.

The dynamical matrix can be derived starting from lattice dynamics. In this theory, the energy of the system as a function of atomic displacement u can be expended through a Taylor perturbation:

$$E = E_0 + \sum_{i,\alpha}\frac{\partial E}{\partial u_{i,\alpha}} + \frac{1}{2}\sum_{i,\alpha,i',\alpha'} u_{i,\alpha}\Phi^{i,i'}_{\alpha,\alpha'}u_{i',\alpha'} + .. \tag{5.3}$$

The subscripts i, α refers to the atom i whose coordinates are α. $\Phi^{i,i'}_{\alpha,\alpha'} = \frac{\partial^2 E}{\partial u_{i,\alpha}\partial u_{i',\alpha'}}$ is the force constant matrix. The demonstration that leads to the dynamical matrix will not be given here but can be found in [49]. The important result is that the

dynamical matrix is the mass reduced Fourier transform of the force constant matrix:

$$D^{i,i'}_{\alpha,\alpha'}(\mathbf{q}) = \frac{1}{\sqrt{m_i m_{i'}}} \sum_i \Phi^{i,i'}_{\alpha,\alpha'} e^{-i\mathbf{q}\mathbf{r}_i} \tag{5.4}$$

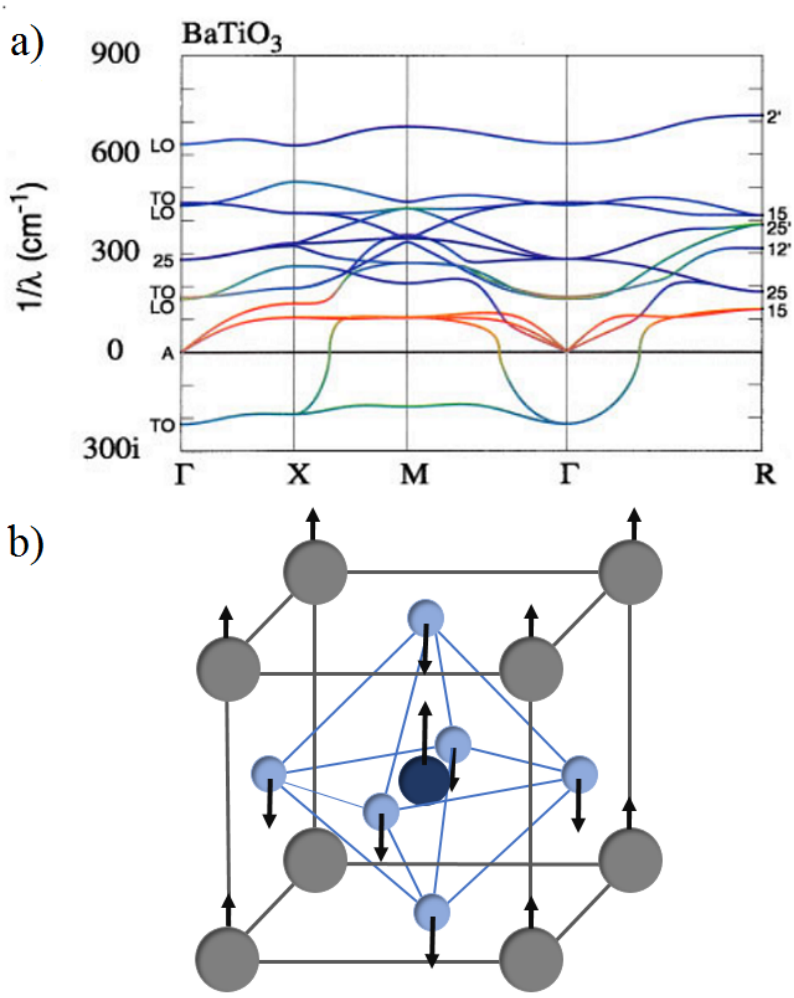

Figure 5.5: a) BaTiO3 phonon dispersion relations obtained from first-principles methods, using the local density approximation to obtain the exchange-correlation [53]. TO and LO stands for transverse and longitudinal optical modes. At Γ, we observe a negative frequency which is the signature of a structural instability. Using the dynamical equation 5.2, one can find the corresponding displacement as shown in b).

5.2 Results and discussion

A property of significant importance in ferroelectricity are the Born effective charges (see Section 2.2.4) which describe the variation of the force on an ion with the change of the electric field. Born effective charges of $BaTiO_3$ are reported in the table 5.1. In combination with the atomic displacement associated to the distortion, they can provide a first estimation of the polarization value. With this approach, a value of 39.55 $\mu C/cm^2$ is obtained which is more than the experimental value (27 $\mu C/cm^2$) but close to other first-principles calculations (36.35 $\mu C/cm^2$ in [54], 47 $\mu C/cm^2$ in [55]). The origin of the difference stands in the value of the ionic displacements and probably comes from different choice of computational parameters. If one calculates the polarization with the ionic displacements obtained using different exchange-correlation functionals, the results would be different since the atomic positions would change. Even for a given exchange-correlation functional, a different DFT code implementation can result in different polarization value. These differences arise from the different level of approximations used to solve the Kohn-Sham equations such as all-electron, PAW or ultrasoft pseudopotentials [56].

Another way to calculate the polarization is to use the Berry phase approach [57], the central result of the modern theory of polarization described in Section 2.2.5. This leads us to a value of 38.43 $\mu C/cm^2$, in good agreement with the Born effective charges calculated value.

Ion	[58]	Cubic	Tetragonal	Displacement ($\mathring{A}$)	Dipole moment ($e\mathring{A}$)
Ba	2.70	2.73	2.89	0.08516	0.2459
Ti	7.10	7.52	4.87	0.1640	0.7986
$O_{\parallel}$	-5.56	-5.99	-4.07	-0.1231	0.5006
$O_{\perp}$	-2.12	-2.13	-1.84	-0.03373	0.06223

Total dipole moment = 1.6695 $e\mathring{A}$
Unit cell volume = 67.53 $\mathring{A}^3$
Polarization = 39.55 $\mu C/cm^2$

Table 5.1: Born effective charges (Z^*_{zz} components) comparison between [58] and calculated values. The displacements of the cubic-to-tetragonal phase transition are also reported.

From the table 5.1, we observe striking differences between the Born effective charges and the ionic charges, especially for Ti (7.52), with a nominal charge of +4, and for $O_{\parallel}$ (-5.99) in its typical -2 oxidation state. Anomalous effective charges are usual in the case of ferroelectric perovskites like $KNbO_3$ [59], $PbZrO_3$ and many other structures [60]. In the case of $BaTiO_3$, a hybridization between the O $2p$ and Ti

$3d$ states, leading to a global charge transfer from the cation to the anion could explain the discrepancy between these values [21]. The difference between the Born effective charges of the cubic and the tetragonal phase are explained by the loss of translational symmetry. In the former, all the Ti-O bond lengths are equal (2.02 $\mathring{A}$) and the resulting Ti-O-Ti-O chain possess a regular interatomic spacing while in the latter, there is an alternation of short (1.82 $\mathring{A}$) and long (2.40 $\mathring{A}$) interatomic distances, thus breaking the Ti-O chain and leading to smaller Born effective charges [21].

Several studies have already been conducted on the origin of the tetragonal deformation in BaTiO3 [61, 62], and have shown the importance of the hybridization of the O $2p$ with the Ti $3d$ states. We reproduce these results by density of states (DOS) calculations. To highlight the effect of the distortion, we use a tetragonal phase with amplified distortion (twice the calculated one) as in ref [61]. Results for the cubic (upper panel) and the tetragonal (lower panel) phase are reported in Fig 5.6. We observe that the occupied valence band has a small Ti character which reflects the hybridization between the O p and Ti d states. Indeed, Ti has a d^0 electronic configuration and should not possesses occupied states. Interestingly, we observe that this hybridization is already present in the cubic phase.

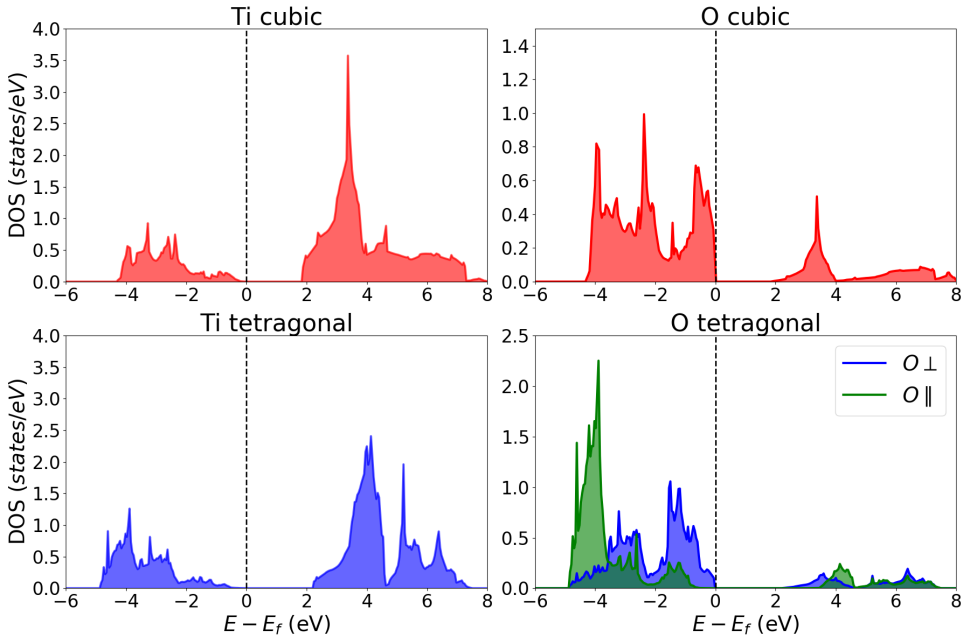

Figure 5.6: In the upper panel, projection of Ti (left) and O (right) DOS in the cubic phase are represented. In the lower panel, projection of Ti (left) and O (right) DOS in a tetragonal phase.

The most interesting change occurs in the O DOS. All O occupy equivalent positions in the perfect octahedron but as soon as it is distorted, we can distinguish the $O_{\parallel}$ (parallel to the direction of the polarization) and the $O_{\perp}$ (perpendicular to the direction of the polarization). The $O_{\parallel}$ displays an enhanced hybridization with a larger energy difference between the valence band states and the conduction band states. The analogy between DOS and molecular orbital diagram is obvious, the stronger the hybridization between atomic orbitals, the larger the energy difference between the molecular orbitals created.

To obtain more insights, a DOS projection over the Ti atomic orbitals is realized (Fig 5.7). With no surprise, we see that most of the changes arising from the hybridization originates from the d_{z^2}, d_{xz} and the d_{yz} orbitals because the distortion is directed along the z axis. The d_{xy} and the $d_{x^2-y^2}$ orbitals, lying in the perpendicular plane, are barely changed.

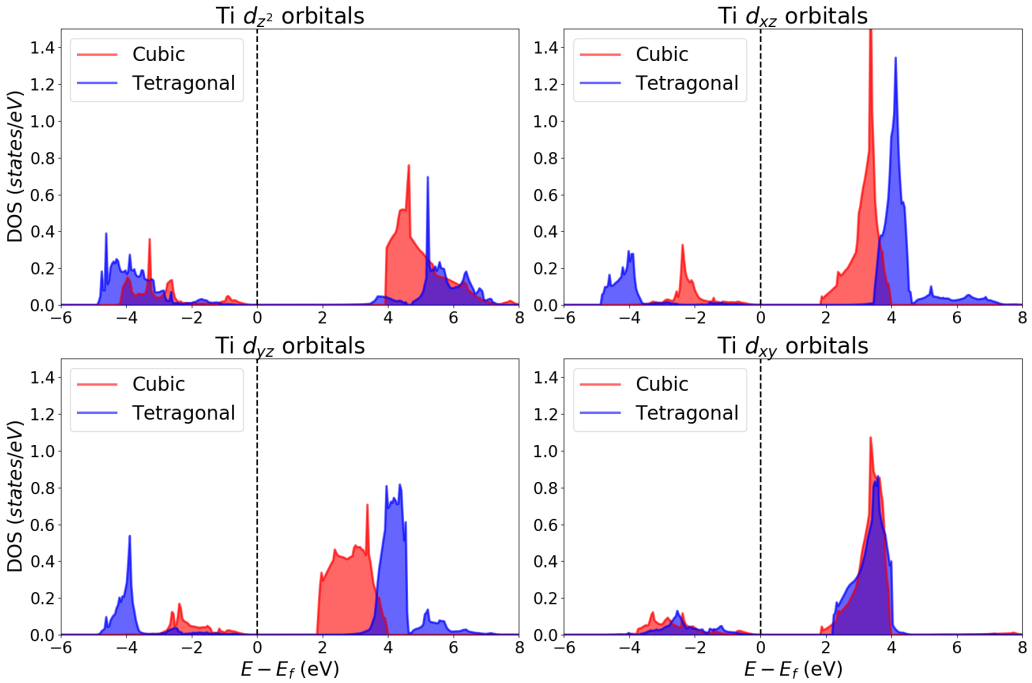

Figure 5.7: DOS projection over the Ti d orbitals. We observe a strong change between the cubic and the tetragonal orbital projected DOS when they possess a z component.

In the solid state, the equilibrium structure can be seen as a delicate compromise between ionic and covalent interactions. For instance, a purely ionic solid with spherical atoms of the same radii would adopt a centrosymmetric structure because it is the most compact arrangement and off-center displacements are severely punished

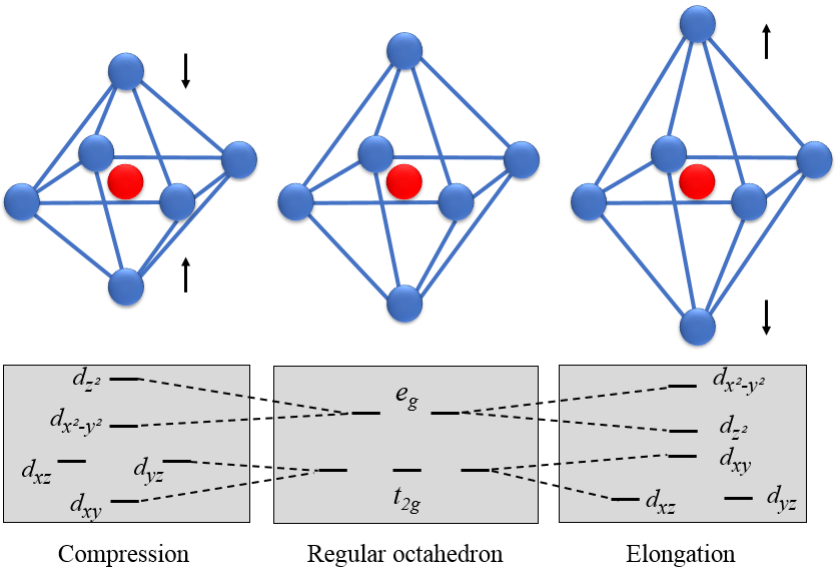

Figure 5.8: The Jahn-Teller distortion in an octahedron complex splits the degenerate terms t_{2g} and e_g into several components.

by the short-range electronic repulsions. Thus, distortion must be associated to covalent effects, *i.e.* chemical bonding must occur to stabilize the distorted structures over the symmetric ones.

This phenomenon is commonly found in the field of molecular chemistry and is known as the Jahn-Teller distortion and states that '*For a nonlinear molecule in a degenerate state, distortion must occur to lower the symmetry, remove the degeneracy, and lower the energy*' [63]. On the Fig 5.8, we can see the splitting of the t_{2g} and e_g states of the center atom upon deformation in the z direction of a regular octahedron. According to the crystal field theory, during compression, d_{xz} and d_{yz} are destabilized because of the rapprochement of the ligands towards the center atom while the other component of the t_{2g}, the d_{xy} is stabilized. The same is true for the e_g states where the d_z^2 will be higher in energy and the $d_{x^2-y^2}$, lower. In the case of the elongation, the orbitals with a z component will be stabilized while the reverse is true for the other orbitals.

All these concepts can be formalized by writing a perturbative expansion of the energy E as a function of the coordinates of the deformation q:

$$E(q) = E(0) + \langle\psi_0|\frac{\partial\hat{H}}{\partial q}|\psi_0\rangle q + \frac{1}{2}\Big(\langle\psi_0|\frac{\partial^2\hat{H}}{\partial q^2}|\psi_0\rangle - 2\sum_n \frac{\langle\psi_0|\frac{\partial\hat{H}}{\partial q}|\psi_n\rangle}{E_0 - E_n}\Big)q^2 \qquad (5.5)$$

$E(0)$ is the energy of the symmetric structure. The second term in this equation is the first order Jahn-Teller effect which accounts for the distortion of molecular complexes described previously. The quadratic term contains two distinctive parts. The first one $\langle\psi_0|\frac{\partial^2\hat{H}}{\partial q^2}|\psi_0\rangle$ corresponds to the increase in energy caused by the coulombic repulsion when the electron clouds are displaced without electronic rearrangements. The second deals with the stabilization energy driven by the formation of new chemical bonds. Two conditions have to be fulfilled in order to make this term consequent. Firstly, the numerator has to be non-zero; this occurs when the ground state ψ_0, corresponding to the symmetric structure, and the distorted state ψ_n have the correct symmetry. Secondly, the denominator $E_0 - E_n$ has to be small; in other words, there must be low-lying free energy states E_n [64]. In $BaTiO_3$, Ti possesses those low lying energy states which allows the strong hybridization with the O p states thus, the denominator of eq. 5.5 is small and the gain of energy is large. In the same time, the term associated to the coulombic repulsion is small because Ti is in a d^0 configuration and overall, the distortion is favored.

Chapter 6

Ba_4Sb_2O

6.1 Phonon dispersion relations

We have seen in $BaTiO_3$ that the ferroelectricity is related to unstable phonon modes which creates a structural instability and results in a phase transition from a paraelectric to a ferroelectric state. This means that new ferroelectric candidates could be identify if their corresponding phonon dispersion relations exhibits negative modes [65]. This methodology was recently applied by our group to a phonon band structure database [66, 67], leading us to a series of potential ferroelectric materials of chemical formula A_4X_2O, where A is an alkaline-earth, X is a trivalent anion. The results of these calculations are shown in Fig 6.1. Whereas the structure with Ba and Sr all exhibit imaginary modes, the ones with Ca are all stable meaning that they will not undergo spontaneous distortion towards a ferroelectric state.

We will focus on the Sb derivatives, Ba_4Sb_2O, Sr_4Sb_2O, Ca_4Sb_2O even if the latter does not possess a ferroelectric distortion. However, structural instabilities lead to several structures, therefore the stability of the ferroelectric phase over these competing phases is not guaranteed. From the energy difference between the different structures (Table 6.1), we found that Ba_4Sb_2O has a ferroelectric stable phase while Sr_4Sb_2O is antiferroelectric.

6.2 Results and discussion

Synthesized for the first time in 1996 by reduction of Sb_2O_3 with Ba [69], Ba_4Sb_2O is a tetragonal ($I4/mmm$) anti-Ruddlesden-Popper phase, a family of general formula

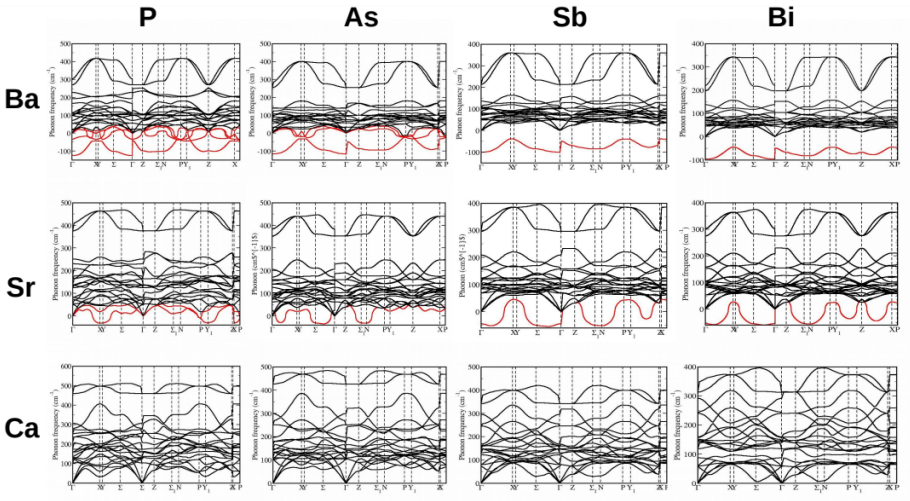

Figure 6.1: Phonons dispersion relations for diverse A_4X_2O compounds. At the exception of Ca, they are all characterized by the presence of imaginary modes, in red, which denotes the instability of these structures [68].

$A_{n-1}A'_2B_nX_{3n+1}$ where n is an integer. Typical examples of Ruddelesden-Popper structures are K_2MgF_4 or K_2NiF_4. They are considered as close successors of the perovskites [70] because they display similar structural features. Ruddlesden-Popper structures can be seen as a sheet-like arrangement of perovskites in the (a,b) plane, stacked in the c direction and each of these slabs are shifted by $(\frac{1}{2}, \frac{1}{2})$ [71]. We define our anti-Ruddlesen-Popper structure by analogy with anti-perovskites such as CuNMn3 or Li3OBr in which cations occupy anionic sites and vice versa. Instead of having a metallic atom in the center of an anionic octahedron, we have an anion, O, inside a cationic octahedron. The structure of Ba_4Sb_2O is shown in Fig 6.2: the octahedrons are slightly distorted which implies that there is two inequivalent positions that we will denote as $Ba_{\parallel}$, parallel to the direction of polarization, and $Ba_{\perp}$, perpendicular to the direction of polarization. The oxygen is located at the center of the octahedrons while the cubic sites are occupied by the Sb atoms.

6.2.1 Ferroelectric distortion

The ferroelectric distortion (Fig 6.3) can be retrieved using the dynamical equation 5.2 and is mainly associated to the off-center displacement of the O from the plane formed by the $Ba_{\perp}$ towards a $Ba_{\parallel}$, the consequence is that we finish in a situation with three distinguishable positions, $Ba_{\parallel}$ close, $Ba_{\parallel}$ far and $Ba_{\perp}$. From now on, the distorted structures will be denoted as child and the original structure as parent, this nomenclature emphasizes the idea that the child structures emerged from a more symmetrical but unstable system, the parent.

The application of the dynamical equation to Ba_4Sb_2O gives several structures which are reported in table 6.1. Most of the children are non-polar, this classification was done simply by taking a look at the space group. From these results, an important comment has to be made, the parent ($I4/mmm$) is the only one that has been synthesized despite being the less stable phase according to our calculations. There are several possible explanations, first we assume a temperature of 0K while the experiments are usually done at room temperature and thus, phase transitions can occur by lowering the temperature. For instance, the energy differences between the cubic (parent) and the children of $BaTiO_3$ are -10.79 meV/at, -13.20 meV/at, -13.76 meV/at for the tetragonal, the orthorhombic and the rhombohedral structures, respectively. The tetragonal phase is stable at room temperature but undergoes a transition to the orthorhombic phase at 278K and then to the rhombohedral phase at 183K. It is also possible that the ferroelectric phase was synthesized but because of an insufficient structure resolution, it was misidentified as non-polar [65]. Indeed, owing to the presence of heavy atoms in the structure (Ba, Sb), the correct position of a light atom such as O can be hard to identify with a powder diffraction experiment. Another explanation would be that the domains are oriented in different directions and the measurement gave the average of all which is the parent.

phase	space group	polar	$\Delta E(meV/at)$
parent	I4/mmm (139)	no	0
child	**I4mm (107)**	**yes**	**-5.897**
child	C2/m (12)	no	-5.297
child	P4/nmm (129)	no	-1.125
child	Cmcm (63)	no	-0.419

Table 6.1: Stability comparison of the different children with respect to the parent

6.2.2 Ferroelectric properties

We have seen in O that Born effective charges could give a good approximation of the value of the polarization using atomic displacements. We have simply repeated the operation, the results of these calculations are shown in table 6.2.

There are several differences between Ba_4Sb_2O and $BaTiO_3$ such as the absence of anomalous effective charges or the amplitude of displacements, which are higher in the first. Overall, the total dipole moments are almost equal since these two opposite trends compensate themselves but because Ba_4Sb_2O has a larger unit cell, the polarization is smaller (11.18 $\mu C/cm^2$) than in $BaTiO_3$ (27 $\mu C/cm^2$ for the tetragonal phase). In comparison, the Berry phase approach gives a value of 7.33

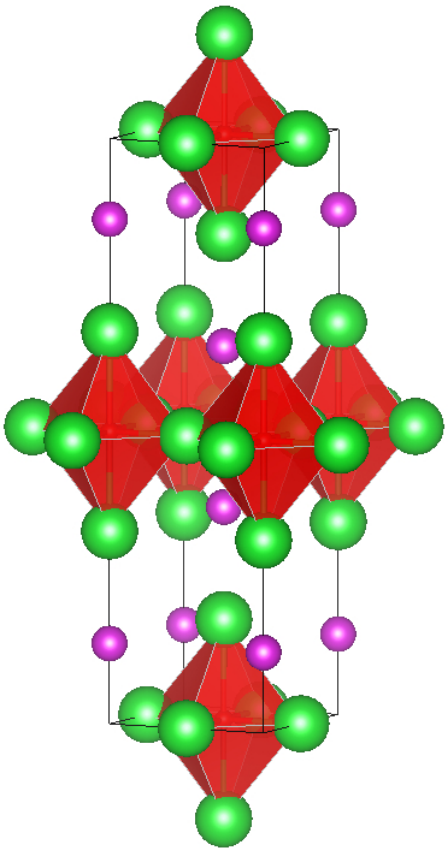

Figure 6.2: Structure of the parent phase of Ba4Sb2O

$\mu C/cm^2$.

Ion	Born effective charges	Displacement ($\AA$)	Dipole moment ($e\AA$)	
$Ba_{\parallel close}$	2.72	0.21	0.57	
$Ba_{\parallel far}$	2.46	0.092	0.23	
$Ba_{\perp far}$	2.49	-0.0084	-0.021	Total
Sb_1	-3.50	-0.0028	-0.0098	
Sb_2	-3.77	0.039	-0.15	
$O_\perp$	-2.90	-0.41	1.19	

dipole moment = 1.82 $e\AA$
Unit cell volume = 261.76 $\AA^3$
Polarization = 11.18 $\mu C/cm^2$

Table 6.2: Born effective charges (Z^*_{zz} components), displacements and dipole moments in Ba4Sb2O. Using these values, the calculated polarization of our material is 11.18 $\mu C/cm^2$

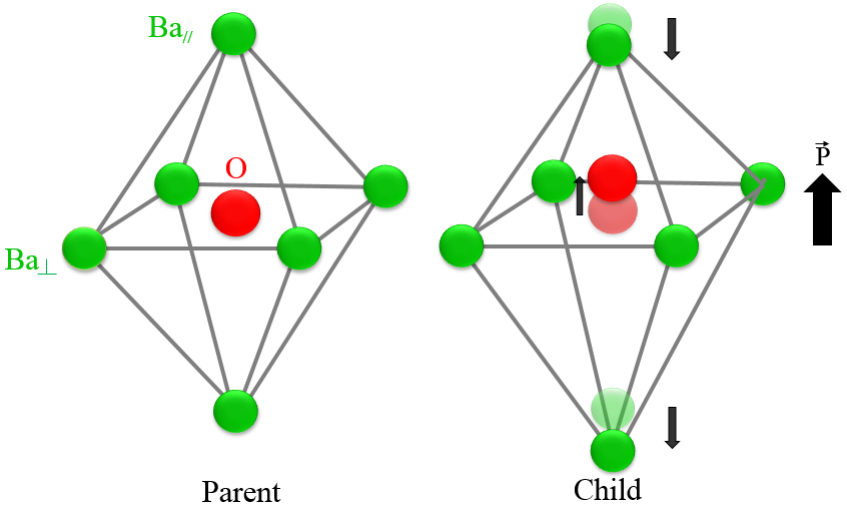

Figure 6.3: Ferroelectric distortion in Ba_4Sb_2O. In the parent, the oxygen is located at the center of a slightly elongated octahedron made up of two inequivalent $Ba_\perp$ and $Ba_\parallel$. The distortion corresponds to the displacement of the O towards a $Ba_\parallel$.

In $BaTiO_3$, we have seen the insights brought by DOS calculations and we will therefore begin our analysis by determining the electronic structure of Ba_4Sb_2O. The results of the projected DOS calculations are shown in Fig 6.4. Like Ti^{4+} in $BaTiO_3$, Ba^{2+} is a close-shell ion, meaning that its valence states are empty. However, because of the hybridization with the p states of O, we observe that the $5d$ states of both Ba are partially occupied. The states above the Fermi level are initially located between -1 eV and -4 eV. After the deformation, they are widened and occupy a region from -1 eV to -6 eV, signature of an enhanced hybridization. Concerning the O, we notice a slight shift in energy upon deformation which also supports the idea of a stronger orbital overlap.

From orbital-resolved DOS calculations, we observe that the main contribution to the hybridization originates from orbitals with a z component as in $BaTiO_3$. However, the effect of the distortion on the DOS is much more important in Ba_4Sb_2O than in $BaTiO_3$ as shown in Fig 6.5. In the left, the orbital-resolved DOS calculations for the d_{z^2} and the d_{yz} orbitals of Ti (unamplified structure) demonstrate that the effect of the hybridization is not so important when compared to Ba in Ba_4Sb_2O (right). This result is not surprising since the displacements in our material are higher than in $BaTiO_3$ leading to larger overlap and thus, to larger hybridization.

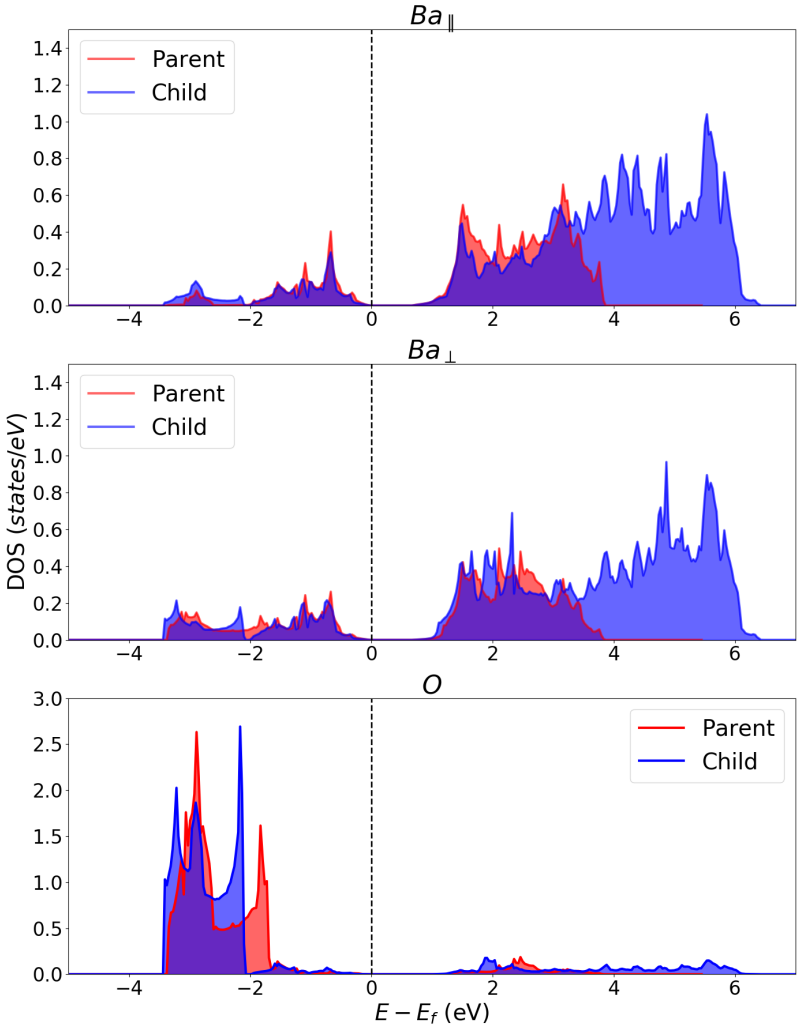

Figure 6.4: Element-resolved DOS for Ba_4Sb_2O. The top panel refers to the projection over the $Ba_{\parallel}$ which becomes $Ba_{\parallel\ close}$ after distortion. In the middle panel, the projection over $Ba_{\perp}$ is shown and finally, the lower panel represents the projection over the O.

6.2.3 Comparison with Ca_4Sb_2O and Sr_4Sb_2O

To understand the role of chemistry in our system, we also investigate the alkaline-earth substitutes of Ba_4Sb_2O: Sr_4Sb_2O, an antiferroelectric, and Ca_4Sb_2O, a paraelectric. The total DOS of the corresponding parent structures are shown in Fig 6.6. We observe that the energy gap between the states is increasing as we substitute Ba for Sr and then for Ca. To formalize that, we use the eq 6.1 to obtain the energetical center of mass of the valence and conduction bands:

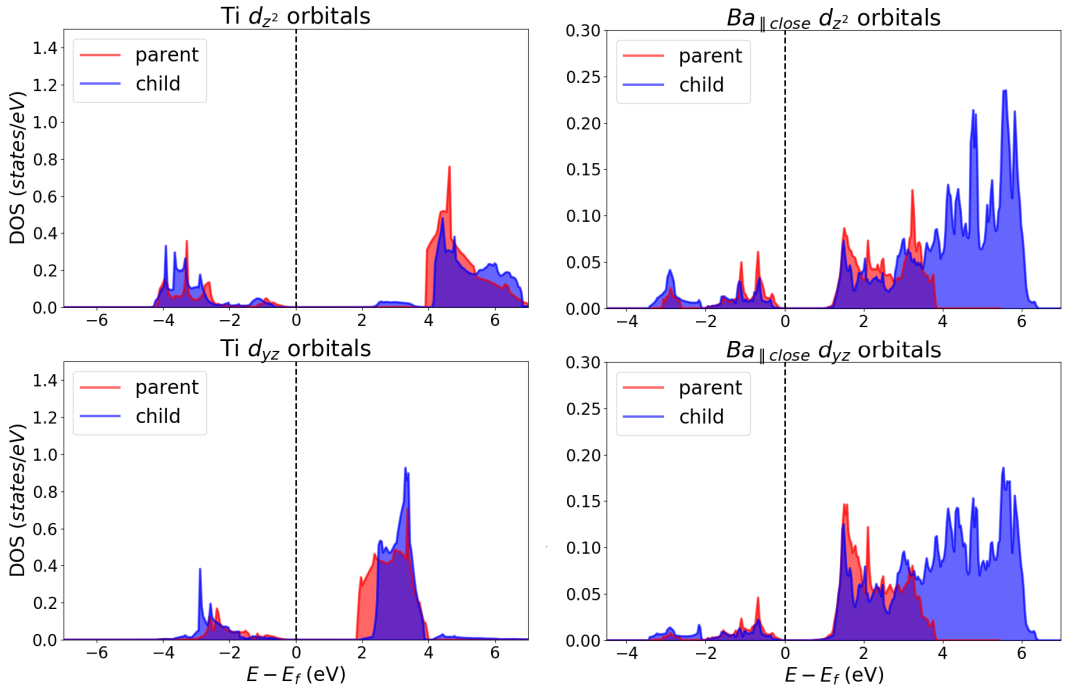

Figure 6.5: Comparison between the orbital-resolved DOS of $BaTiO_3$ (left) and Ba_4Sb_2O (right).

$$E_{CoM} = \frac{\sum_i DOS(E_i)E_i}{\sum_i E_i} \tag{6.1}$$

The energy differences between the center of mass of the valence band and the conduction bands are 4.21 eV, 5.79 eV and 6.88 eV for Ba_4Sb_2O, Sr_4Sb_2O and Ca_4Sb_2O, respectively. We can understand these different behaviors using eq 5.5, small energy gap between unoccupied and occupied states are necessary to compensate the cost associated to the increasing coulombic repulsion upon distortion. This condition is comparable to the situation in diatomic molecules, where small energy difference leads to a better stability. The smallest energy gap is found in Ba_4Sb_2O and it is therefore the only one to possess a stable ferroelectric phase. In the opposite, Ca_4Sb_2O have the largest energy gap of the series and thus, the chemical bond formation does not compensate the increasing coulombic repulsion and overall, Ca_4Sb_2O is paraelectric. Finally, Sr_4Sb_2O and its intermediate band gap is neither paraelectric nor ferroelectric but antiferroelectric.

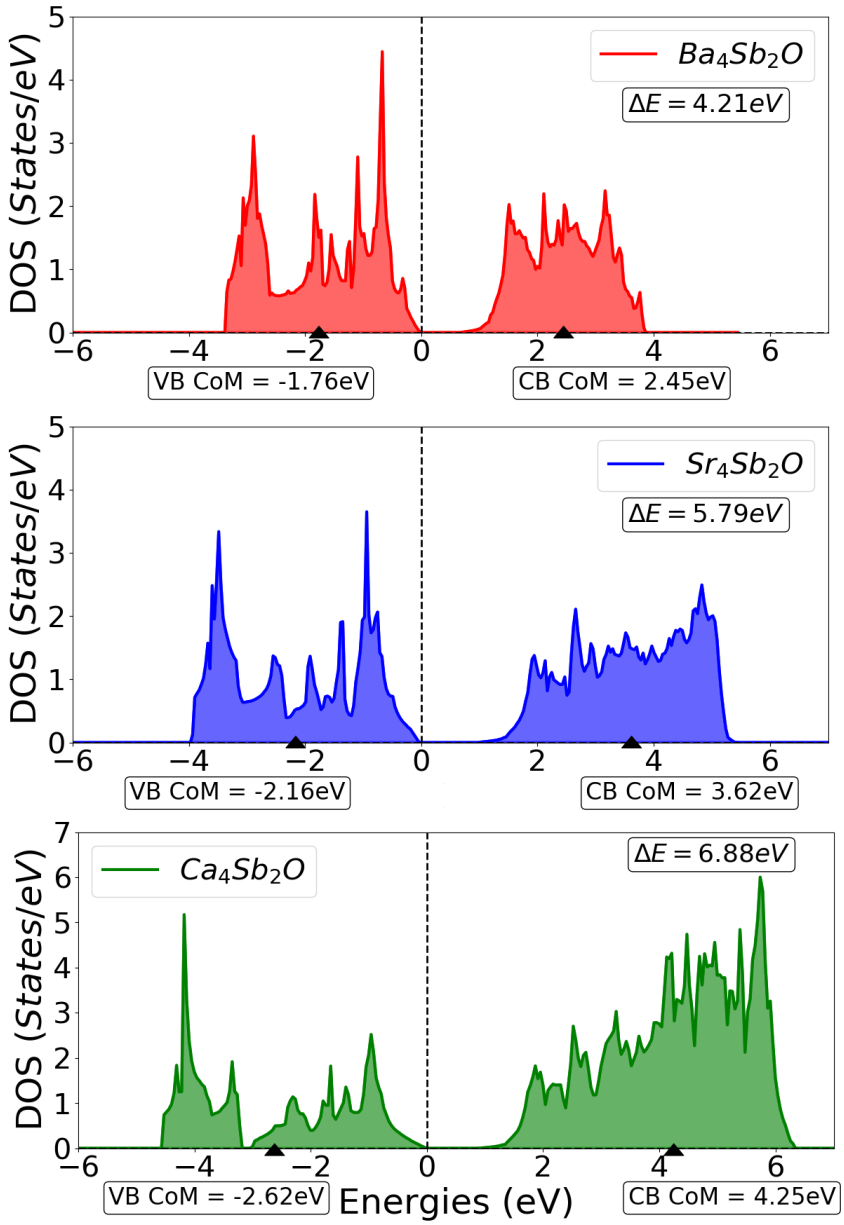

Figure 6.6: Comparison of the DOS for A_4Sb_2O where A is either Ca, Sr or Ba, the valence band has its energetical center of mass (eq 6.1) lowered in energy when moving towards heavier alkaline-earth. The opposite trend is observed for the conductive band which is higher in energy along the row of the periodic table.

6.2.4 COHP analysis

The basis sets used in the study of solid state and of molecular system are rather different. Whereas the linear combination of atomic orbitals (LCAO) approach is usually preferred in quantum chemistry, the presence of periodic boundary conditions naturally leads to choose plane-waves as the basis sets to describe the electronic structure.

This method is very powerful since the description of the whole basis can be controlled by only one parameter, the cut-off energy. However, the cost to pay is that all the chemical information about bonds, atomic charge, etc. is lost. The Crystal Orbital Hamilton Population (COHP) method provides a way to project the plane-waves into a localized basis sets to recover all these insights [72].

To support the idea that the displacement is linked to a chemical bond formation, a COHP analysis was performed [47]. The results are shown in table 6.3. The energy gain brought by the movement of O towards a Ba$_\parallel$ is -62.7 meV and the distance between the two atoms is shortened by 0.63 $\mathring{A}$ while the other Ba$_\parallel$ has its bond length with O elongated by 0.50 $\mathring{A}$ and lose -77.1 meV in comparison with the parent structure.

Ba_4Sb_2O	$ICOHP_{parent}(eV)$	$ICOHP_{child}(eV)$
$Ba_{\parallel close}O$	-0.26664	-0.32935
$Ba_{\parallel far}O$	-0.26664	-0.18945
$Ba_{\perp close}O$	-0.35737	-0.35402

Table 6.3: ICOHP analysis of Ba_4Sb_2O [68]

6.2.5 Strain analysis

The growth of a thin-film material on a substrate of different lattice parameters can result in strain and this can lead to important changes between the intrinsic properties material and its strained counterpart. This methodology was successfully applied to the field of ferroelectricity. For instance, $BaTiO_3$ thin-film were grown on $GdScO_3$ or $DyScO_3$ leading to compressive in-plane strain of -1 % and -1.7 %, respectively, which raise the Curie temperature by about 300K and increase the polarization by 270 % [73]. More recently, theoretical calculations have shown that ferroelectricity could be brought by epitaxial strain in binary alkaline-earth oxides such as MgO, CaO or BaO [74].

To study the effect of strain on Ba4Sb2O ferroelectric child and parent, we applied a strain in the a, b plane and in the c direction from -5 % to +5 % by interval of 1 %. In total, 121 structures were calculated for each phase. The results of these calculations are shown in Fig 6.7. From this, we see that both parent and child exhibit the same trends. The structures are destabilized at high strain, compressive or tensile, the energetic minimum being the unstrained structure. Interestingly, when a compressive strain is applied in one direction, the energy minima lies in the region of tensile strain for the other direction and reversely.

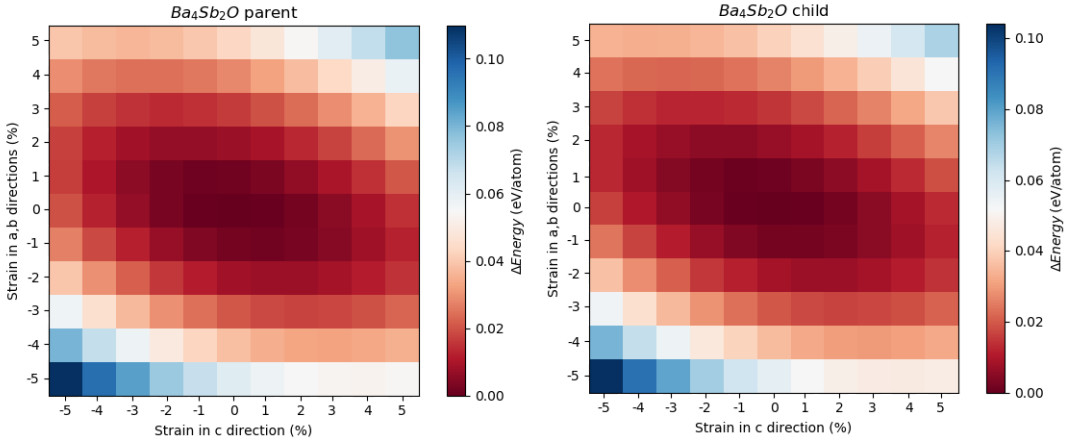

Figure 6.7: ΔE as a function of the strain applied in the a, b plane and in the c direction. The references are the unstrained structures.

During an epitaxial experiment, two parameters can be controlled. The magnitude of the strain applied depends on the lattice parameters of the substrate. For smaller lattice constants, the thin-film will be compressed and inversely, if the lattice constants are higher, the thin-film will be elongated. Also, the orientation of the growth can be chosen to only tune one parameter at the time. For instance, if the thin-film growth is directed towards [001], strain can only be applied in the a, b plane.

Here, we considered that only the strain in the a, b plane could be controlled. Therefore, we looked at the energetic minimum in c corresponding to each a (since a=b), the results are plotted in Fig 6.8 a) for both parent and child. Since the lattice parameter of the two structures are different, we applied a polynomial regression up to the 4th degree:

$$E = \alpha_0 + \alpha_1 x + \alpha_2 x^2 + \alpha_3 x^3 + \alpha_4 x^4 \tag{6.2}$$

Then, the difference between the two polynomial functions was plotted as a function of the lattice strain of the child. The polarization associated to each of the calculated

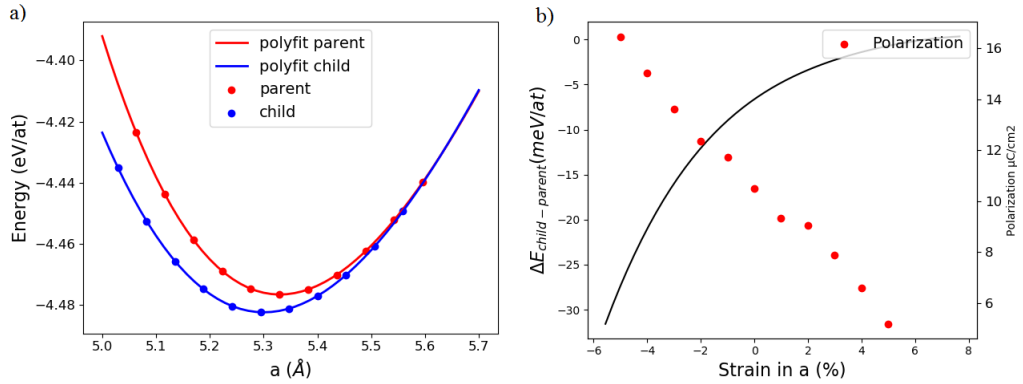

Figure 6.8: a) Energetic minima associated to each applied strain in the a, b plane (since $a = b$, we didn't indicate b). A polynomial regression was realized to allow a comparison between the parent and child. b) The black line shows the energy difference between parent and child. The red dots shows the polarization associated. When a compressive strain is applied, the child is stabilized over the parent while the associated polarization is increasing.

structures was then calculated using the Born effective charges of the child structure (see Fig 6.8 b).

From Fig 6.8, we see that the application of a compressive strain results in the stabilization of the child phase over the parent phase and in the increase of the polarization. Starting from a situation where $\mathbf{P} = 10.59\ \mu C/cm^2$, $\mathbf{P}$ can be enhanced up to 13.60 $\mu C/cm^2$ for a strain of -3 %. In the same time, this would increase the energy difference between the parent and the child from ΔE = -5.90 meV/at to ΔE = -16.28 meV/at. In comparison, the theoretical energy difference between $BaTiO_3$ (T_c=393K) and $PbTiO_3$ (T_c=760K) paraelectric and ferroelectric phase is -11.2 meV/at and 41 meV/at [55]. We can reasonably suppose that increasing the stability of the child over the parent will lead to a higher T_c. This would be of great interest if the T_c of the unstrained Ba_4Sb_2O is below room temperature.

Chapter 7

Conclusion

Ferroelectrics are an important class of materials characterized by the existence of two stable polar states switchable by the application of an electric field. They share many similarities with ferromagnetic materials such as hysteresis loop, the presence of domains or the existence of a Curie temperature, temperature at which the spontaneous polarization disappears. In magnetoelectric multiferroic materials, both ferroelectricity and ferromagnetism are present in the same phase. This allows the possibility to control magnetic properties with electric field and inversely, giving rise to multiple applications.

The field of electronic could greatly benefits from ferroelectric materials. Indeed, they are used as basic components to create energy-efficient devices such as negative capacitors or as memory element in ferroelectric random-access memory (FeRAM). The coupling with magnetism in magnetoelectric materials leads to further applications such as magnetoelectric spin-orbital (MESO) logic devices. This technology could eventually outshine the complementary metal-oxide semiconductors (CMOS) on which most of our electronic devices currently relies.

The development of new ferroelectric materials requires a deeper knowledge on their fundamental properties. In this master thesis, we have studied $BaTiO_3$ a well-known ferroelectric material and showed that a hybridization between the O $2p$ and the Ti $3d$ states was responsible for the ferroelectric deformation. The hybridization can be seen from DOS analysis where the distortion leads to the splitting of the orbitals. Using a perturbative expansion, we showed that the off-centering could be associated to a second-order Jahn-Teller distortion.

A study of a new ferroelectric candidate Ba_4Sb_2O was then realized. This anti-

perovskite structure was identified from the presence of unstable phonon modes. As for $BaTiO_3$, a second-order Jahn-Teller distortion appears to be the origin of the displacement of the O from the center of the octahedron towards a Ba. More precisely, the off-centering is associated to a hybridization between the O $2p$ and the Ba $5d$ states. Furthermore, using a perturbative expansion of the energy as a function of the displacement coordinates, we showed that the different behaviors of ferroelectric Ba_4Sb_2O, antiferroelectric Sr_4Sb_2O and paraelectric Ca_4Sb_2O could be understood in term of energy gaps between the conductive states and the valence states. The larger the gap is, the less strong the hybridization is. Finally, the strain analysis of Ba_4Sb_2O showed that the stability of the ferroelectric phase could be enhanced as well as the polarization by a compressive strain. This could be achieved by an epitaxial growth of Ba_4Sb_2O on a substrate with smaller lattice constants.

A_4X_2O are a promising family and deserves more attention in the future. In this master thesis, we focus ourselves in the study of the structures where $X = Sb$ but other members of the A_4X_2O can be investigated in the future. Furthermore, there is a possibility to render the structure magnetoelectric by incorporating a divalent lanthanide. For instance, Eu_4Sb_2O exhibits a ferromagnetic ground-state making it a interesting magnetoelectric candidate.

Bibliography

[1] G. E. Moore. Cramming more components onto integrated circuits. *Electronics*, 38, 1965.

[2] R. R. Schaller. Moore's law: past, present and future. *IEEE Spectrum*, 34:52–59, 1997.

[3] Van Heddeghem W., Lambert S., Lannoo B., Colle D., Pickavet M., and Demeester P. Trends in worldwide ict electricity consumption from 2007 to 2012. *Computer Communications*, 50:64 – 76, 2014.

[4] A. S. G. Andrae and T. Edler. On global electricity usage of communication technology: Trends to 2030. *Challenges*, 6:117–157, 2015.

[5] D. Damjanovic, P. Muralt, and N. Sette. Ferroelectric sensors. *IEEE Sensors Journal*, 1:191–206, 2001.

[6] N. A. Spaldin and M. Fiebig. The renaissance of magnetoelectric multiferroics. *Science*, 309:391–392, 2005.

[7] S. Manipatruni, D. E. Nikonov, C-C. Lin, T. A. Gosavi, H. Liu, B. Prasad, Y-L. Huang, E. Bonturim, R. Ramesh, and I. A. Young. Scalable energy-efficient magnetoelectric spin–orbit logic. *Nature*, 565:35–42, 2019.

[8] K. M. Rabe, C. H. Ahn, and J-M. Triscone. *Physics of Ferroelectrics: A Modern Perspective*. 1st edition, 2007.

[9] C. Kittel and J.K. Galt. Ferromagnetic domain theory. volume 3 of *Solid State Physics*, pages 437 – 564. Academic Press, 1956.

[10] A. Arora. *Optical and electric field control of magnetism*. PhD thesis, 01 2018.

[11] J. Valasek. Piezo-electric and allied phenomena in rochelle salt. *Phys. Rev.*, 17:475–481, 1921.

[12] J. Valasek. The early history of ferroelectricity. *Ferroelectrics*, 2:239–244, 1971.

[13] G-M. Rignanese. Physics of functional materials - LMAPR2014.

[14] N. A. Spaldin. A beginner's guide to the modern theory of polarization. *Journal of Solid State Chemistry*, 195:2 – 10, 2012.

[15] M Stewart, M. Cain, and D. Hall. Ferroelectric hysteresis measurement and analysis. *Report CMMT (A)*, 152, 1999.

[16] S. Horiuchi and Y. Tokura. Organic ferroelectrics. *Nature Materials*, 7:357–366, 2008.

[17] A. K. Tagantsev, K. Vaideeswaran, S. B. Vakhrushev, and et al. The origin of antiferroelectricity in PbZrO3. *Nature Communications*, 4(1):2229, Jul 2013.

[18] P. Vilarinho. *Functional Materials: Properties, Processing and Applications*, volume 186, pages 3–33. 01 2005.

[19] K. M. Rabe. *Antiferroelectricity in Oxides: A Reexamination*, chapter 7, pages 221–244. John Wiley and Sons, Ltd, 2013.

[20] J. Guyonnet. *Domain Walls in Ferroelectric Materials*, pages 7–24. 2014.

[21] Ph. Ghosez, X. Gonze, Ph. Lambin, and J.-P. Michenaud. Born effective charges of barium titanate: Band-by-band decomposition and sensitivity to structural features. *Phys. Rev. B*, 51:6765–6768, 1995.

[22] R. D. King-Smith and D. Vanderbilt. Theory of polarization of crystalline solids. *Physical Review B*, 47:1651–1654, 1993.

[23] N. A. Hill. Why are there so few magnetic ferroelectrics? *The Journal of Physical Chemistry B*, 104:6694–6709, 2000.

[24] J. Wang, J. B. Neaton, H. Zheng, V. Nagarajan, S. B. Ogale, B. Liu, D. Viehland, V. Vaithyanathan, D. G. Schlom, U. V. Waghmare, N. A. Spaldin, K. M. Rabe, M. Wuttig, and R. Ramesh. Epitaxial bifeo3 multiferroic thin film heterostructures. *Science*, 299(5613):1719–1722, 2003.

[25] J. H. Lee and et al. A strong ferroelectric ferromagnet created by means of spin–lattice coupling. *Nature*, 466:954–958, 2010.

[26] M. Jing, H. Jiamian, L. Zheng, and N. Ce-Wen. Recent progress in multiferroic magnetoelectric composites: from bulk to thin films. *Advanced Materials*, 23:1062–1087, 2011.

[27] D. A. Sanchez and et al. Room-temperature single phase multiferroic magnetoelectrics: $Pb(Fe,M)x(Zr,Ti)(1\text{-}x)O3$ [M=Ta, Nb]. *Journal of Applied Physics*, 113:074105, 2013.

[28] I. Bhati, M. Chang, Chishti Z., S. Lu, and B. Jacob. Dram refresh mechanisms, penalties, and trade-offs. *IEEE Transactions on Computers*, 65:108–121, 2016.

[29] K. Iniewski. *CMOS Processors and Memories*. 2010.

[30] D. Bondurant. Ferroelectronic ram memory family for critical data storage. *Ferroelectrics*, 112:273–282, 1990.

[31] Philip Ball. Technology takes tiny steps. *Nature Materials*, 6:182–182, 2007.

[32] C-P. Yeh, M. Lisker, B. Kalkofen, and E. P. Burte. Fabrication and investigation of three-dimensional ferroelectric capacitors for the application of feram. *AIP Advances*, 6:035128, 2016.

[33] Th. Mikolajick, S. Slesazeck, M. H. Park, and U. Schroeder. Ferroelectric hafnium oxide for ferroelectric random-access memories and ferroelectric field-effect transistors. *MRS Bulletin*, 43:340–346, 2018.

[34] V. V. Zhirnov and R. K. Cavin. Negative capacitance to the rescue? *Nature Nanotechnology*, 3:77–78, 2008.

[35] S. Salahuddin and S. Datta. Use of negative capacitance to provide voltage amplification for low power nanoscale devices. *Nano Letters*, 8:405–410, 2008. PMID: 18052402.

[36] A. I. Khan, K. Chatterjee, B. Wang, S. Drapcho, L. You, C. Serrao, S. R. Bakaul, R. Ramesh, and S. Salahuddin. Negative capacitance in a ferroelectric capacitor. *Nature Materials*, 14:182–186, 2015.

[37] A. I. Khan. On the microscopic origin of negative capacitance in ferroelectric materials: A toy model. In *2018 IEEE International Electron Devices Meeting (IEDM)*, pages 9.3.1–9.3.4, 2018.

[38] T. Zhao, A. Scholl, F. Zavaliche, K. Lee, M. Barry, A. Doran, M. P. Cruz, Y. H. Chu, C. Ederer, N. A. Spaldin, R. R. Das, D. M. Kim, S. H. Baek, C. B. Eom, and R. Ramesh. Electrical control of antiferromagnetic domains in multiferroic bifeo3 films at room temperature. *Nature Materials*, 5(10):823–829, 2006.

[39] J. T. Heron, J. L. Bosse, Q. He, Y. Gao, M. Trassin, L. Ye, J. D. Clarkson, C. Wang, Jian Liu, S. Salahuddin, D. C. Ralph, D. G. Schlom, J. Íñiguez, B. D. Huey, and R. Ramesh. Deterministic switching of ferromagnetism at room temperature using an electric field. *Nature*, 516:370–373, 2014.

[40] S. C. McBain, H. H. P. Yiu, and Jon Dobson. Magnetic nanoparticles for gene and drug delivery. *International journal of nanomedicine*, 3:169–180, 2008.

[41] J. Dobson. Magnetic nanoparticles for drug delivery. *Drug Development Research*, 67:55–60, 2006.

[42] N. A. Spaldin. Multiferroics beyond electric-field control of magnetism. *Proceedings of the Royal Society A: Mathematical, Physical and Engineering Sciences*, 476:20190542, 2020.

[43] H. Abd El Azim. Magneto-electric nanocarriers for drug delivery: An overview. *Journal of Drug Delivery Science and Technology*, 37:46 – 50, 2017.

[44] G. Kresse and J. Furthmuller. Efficient iterative schemes for ab initio total-energy calculations using a plane-wave basis set. *Phys. Rev. B*, 54:11169–11186, 1996.

[45] P. E. Blochl. Projector augmented-wave method. *Phys. Rev. B*, 50:17953–17979, 1994.

[46] J. P. Perdew, K. Burke, and M. Ernzerhof. Generalized gradient approximation made simple. *Phys. Rev. Lett.*, 77:3865–3868, Oct 1996.

[47] R. Dronskowski and P. E. Bloechl. Crystal orbital hamilton populations (cohp): energy-resolved visualization of chemical bonding in solids based on density-functional calculations. *The Journal of Physical Chemistry*, 97(33):8617–8624, 1993.

[48] A. von Hippel. Ferroelectricity, domain structure, and phase transitions of barium titanate. *Rev. Mod. Phys.*, 22:221–237, 1950.

[49] James Patterson and Bernard Bailey. *Solid State Physics: Introduction to the Theory.* 3 edition, 2018.

[50] G. Hautier. Chimie-physique et calculs physico-chimique, LCHM2150.

[51] W. Cochran. Crystal stability and the theory of ferroelectricity. *Advances in Physics*, 9:387–423, 1960.

[52] Y. Luspin, J. L. Servoin, and F. Gervais. Soft mode spectroscopy in barium titanate. *Journal of Physics C: Solid State Physics*, 13:3761–3773, 1980.

[53] Ph. Ghosez, E. Cockayne, U. V. Waghmare, and K. M. Rabe. Lattice dynamics of BaTio3, PbTio3, PbZrO3 : A comparative first-principles study. *Physical Review B*, 60:836–843, 1999.

[54] Ph. Ghosez. *First-principles study of the dielectric and dynamical properties of BaTiO3.* PhD thesis, Universite Catholique de Louvain, 1997.

[55] Y. Zhang, J. Sun, J. P. Perdew, and X. Wu. Comparative first-principles studies of prototypical ferroelectric materials by LDA, GGA, and SCAN meta-GGA. *Phys. Rev. B*, 96:035143, 2017.

[56] Kurt Lejaeghere and et al. Reproducibility in density functional theory calculations of solids. *Science*, 351(6280), 2016.

[57] R. D. King-Smith and D. Vanderbilt. Theory of polarization of crystalline solids. *Phys. Rev. B*, 47:1651–1654, 1993.

[58] Ph. Ghosez, X. Gonze, and J. P. Michenaud. First principle calculations of dielectric and effective charge tensors in barium titanate. *Ferroelectrics*, 153:91–96, 1994.

[59] R. Resta, M. Posternak, and A. Baldereschi. Towards a quantum theory of polarization in ferroelectrics: The case of KNbO3. *Phys. Rev. Lett.*, 70:1010–1013, 1993.

[60] W. Zhong, R. D. King-Smith, and D. Vanderbilt. Giant lo-to splittings in perovskite ferroelectrics. *Phys. Rev. Lett.*, 72:3618–3621, 1994.

[61] A. Filippetti and N. A. Hill. Coexistence of magnetism and ferroelectricity in perovskites. *Phys. Rev. B*, 65:195120, 2002.

[62] R. Cohen. Origin of ferroelectricity in perovskite oxides. *Nature*, 358:136–138, 1992.

[63] James E. Huheey, Ellen A. Keiter, and Richard L. Keiter. Inorganic chemistry: principles of structure and reactivity, 4th ed. *Journal of Chemical Education*, 70, 1993.

[64] J. K. Burdett. Use of the jahn-teller theorem in inorganic chemistry. *Inorganic Chemistry*, 20:1959–1962, 1981.

[65] K. F. Garrity. High-throughput first-principles search for new ferroelectrics. *Phys. Rev. B*, 97:024115, 2018.

[66] A. Jain, S. P. Ong, G. Hautier, W. Chen, W. D. Richards, S. Dacek, S. Cholia, D. Gunter, D. Skinner, G. Ceder, and K. a. Persson. The Materials Project: A materials genome approach to accelerating materials innovation. *APL Materials*, 1(1):011002, 2013.

[67] G. Petretto, S. Dwaraknath, H. P.C. Miranda, D. Winston, M. Giantomassi, M. J. van Setten, X. Gonze, K. A. Persson, G. Hautier, and G-M. Rignanese. High-throughput density-functional perturbation theory phonons for inorganic materials. *Scientific Data*, 5(1):180065, 2018.

[68] M. Markov, L. Alaerts, H. Miranda, G. Petretto, C. Wei, J. George, Ph. Ghosez, E. Bousquet, G.M. Rignanese, and G. Hautier. Ferroelectricity and multiferroicity through anion displacement in anti-ruddlesen-popper structures. 2020.

[69] C. Röhr and R. George. Crystal structure of barium antimonide oxide, Ba4Sb2O. *Zeitschrift für Kristallographie - Crystalline Materials*, 211:478 – 478, 1996.

[70] Aleksandrov K.S. Beznosikov, B.V. Perovskite-like crystals of the ruddlesden-popper series. *Crystallogr. Rep.*, 45:792–798, 2000.

[71] I. B. Sharma and B. Singh. Solid state chemistry of ruddlesden-popper type complex oxides. *Bulletin of Materials Science*, 21:363–374, 1998.

[72] V. L. Deringer, A. L. Tchougréeff, and R. Dronskowski. Crystal orbital hamilton population (cohp) analysis as projected from plane-wave basis sets. *The Journal of Physical Chemistry A*, 115:5461–5466, 2011.

[73] K-J. Choi and et al. Enhancement of ferroelectricity in strained BaTiO3 thin films. *Science*, 306:1005–1009, 2004.

[74] E. Bousquet, N. A. Spaldin, and Ph. Ghosez. Strain-induced ferroelectricity in simple rocksalt binary oxides. *Phys. Rev. Lett.*, 104:037601, 2010.

UNIVERSITÉ CATHOLIQUE DE LOUVAIN
Faculté des sciences
Place des sciences, 2 bte L6.06.01, 1348 Louvain-la-Neuve, Belgique | **www.uclouvain.be/sc**